Transcriptional circuitry of NKX2-1 and SOX1 defines an unrecognized lineage subtype of small cell lung cancer

Ranran Kong[1,2,3], Ayushi S. Patel[2,3,4], Takashi Sato[2,3,5], Seungyeul Yoo[6,7], Li Bao[8], Abhilasha Sinha[2,3], Feng Jiang[2,3], Yang Tian[2,3], Maya Fridrikh[2,3], Shuhui Liu[9], Jie Feng[10], Xijing He[11,12], Jiantao Jiang[1], Yuefeng Ma[1], Karina Grullon[2,3], Dawei Yang[2,3,13], Charles A. Powell[2,3], Mary Beth Beasley[14], Jun Zhu[3,6,7], Eric L. Snyder[15,16], Shaomin Li[1]*, and Hideo Watanabe[2,3,6]*

[1]Department of Thoracic Surgery, The Second Affiliated Hospital of Medical School, Xi'an Jiaotong University, Xi'an, Shaanxi, 710004, China;

[2]Division of Pulmonary, Critical Care and Sleep Medicine, Department of Medicine, Icahn School of Medicine at Mount Sinai, New York, NY 10029, USA;

[3]Tisch Cancer Institute, Icahn School of Medicine at Mount Sinai, New York, NY 10029, USA;

[4]Division of Hematology & Medical Oncology, Laura and Isaac Perlmutter Cancer Center, New York University Langone Medical Center, New York, NY, USA;

[5]Department of Respiratory Medicine, Kitasato University School of Medicine, Sagamihara, Japan; Division of Pulmonary Medicine, Department of Medicine, Keio University School of Medicine, Tokyo, Japan;

[6]Department of Genetics and Genomic Sciences, Icahn School of Medicine at Mount Sinai, New York, NY 10029, USA;

[7]Sema4, a Mount Sinai venture, Stamford, CT 06902, USA;

[8]Ningxia People's Hospital, Yinchuan, Ningxia Province, 750001, China;

[9]Division of Infectious Diseases, Department of Medicine, Icahn School of Medicine at Mount Sinai, New York, NY 10029, USA;

[10]Department of Nephrology, The First Affiliated Hospital of Medical School, Xi'an Jiaotong University, Xi'an, Shaanxi, 710061, China;

[11]Department of Orthopedics, The Second Affiliated Hospital of Medical School, Xi'an Jiaotong University, Xi'an, Shaanxi, 710004, China;

[12]Xi'an International Medical Center, Xi'an, Shaanxi, 710126, China;

[13]Department of Pulmonary and Critical Care Medicine, Zhongshan Hospital Fudan University, Shanghai, 200032, China;

[14]Department of Pathology and Laboratory Medicine, Icahn School of Medicine at Mount Sinai, New York, NY 10029, USA;

[15]Department of Pathology, University of Utah, Salt Lake City, UT 84112; Department of Oncological Sciences, University of Utah, Salt Lake City, UT 84112, USA;

[16]Huntsman Cancer Institute, University of Utah, Salt Lake City, UT 84112

* Both authors share senior authorship.

H.W. has been supported by ATS Foundation Unrestricted Grant (ATS-2017-24), the American Lung Association of the Northeast Lung Cancer Discovery Award (LCD-504985), Department of Defense (W81XWH-19-1-0613) and NIH (R01CA240342). R.K. is supported by Shaanxi Provincial Natural Science Foundation, China (2017JM8046). T. S. is supported by the Japanese Respiratory Society, the 6th Lilly Oncology Fellowship Program, and the Uehara Memorial Foundation. J. F. is supported by National Natural Science Foundation of China (NSFC) (No. 82100718). D. Y. is supported by Shanghai Pujiang Program (20PJ1402400). C.A.P. and H. W. are supported by NIH (R01CA163772). E.L.S. is supported by the NIH (R01CA212415, R01CA240317) and the American Lung Association Lung Cancer Discovery Award (LCD-821670). This work was supported in part through the computational resources and staff expertise provided by Scientific Computing at the Icahn School of Medicine at Mount Sinai.

Correspondence and requests for reprints should be addressed to Hideo Watanabe, Division of Pulmonary, Critical Care and Sleep Medicine, Department of Medicine, Icahn School of Medicine at Mount Sinai, New York, NY 10029, USA. Phone: 212-241-9242; Fax: 212-876-5519; Email: hideo.watanabe@mssm.edu.

Author contributions: Conceptualization & Methodology, R.K., and H.W.; Data Collection: R.K., A.S.P., T.S., S.Y., L.B., F.J., M.F., S.L., J.F., X.H., J.J., Y.M., K.G., D.Y., E.L.S., S.L., L.S., and H.W.; Resources, E.L.S., M.B.B., C.A.P., S.L., and H.W.; Data Analysis, R.K., S.Y., A.S.P., S.L., M.B.B., E.L.S., and H.W.; Writing – Original Draft, R.K., A.S.P. and H.W.; Writing-Review & Editing, R.K., A.S.P., E.L.S., and H.W.; Supervision, C.A.P., J.Z. S.L., and H.W.; Project Administration & Funding Acquisition, H.W.

Running title: Collaboration of NKX2-1 and SOX1 defines SCLC-A1 subtype

Descriptor number: 9.26 Lung Cancer: Cellular and Molecular Aspects

The total word count for the body of the manuscript: 3,500

This article has an online data supplement, which is accessible from this issue's table of content online at www.atsjournals.org

Abstract:

Rationale: The current molecular classification of small cell lung cancer (SCLC) based on expression of four lineage transcription factors still leaves its major subtype SCLC-A as a heterogeneous group, necessitating more precise characterization of lineage subclasses.

Objectives: To refine the current SCLC classification with epigenomic profiles and to identify features of the re-defined SCLC subtypes.

Methods: We performed unsupervised clustering of epigenomic profiles on 25 SCLC cell lines. Functional significance was evaluated by cell growth, apoptosis and xenograft using CRISPR-Cas9-mediated deletion. The specific cistromic profiles by ChIP-seq and its functional transcriptional partners using co-immunoprecipitation followed by mass spectrometry were determined. *Rb1*$^{fl/fl}$*Trp53*$^{fl/fl}$ and *Rb1*$^{fl/fl}$*Trp53*$^{fl/fl}$*Nkx2-1*$^{fl/fl}$ mouse models were engineered to explore the function of *Nkx2-1* in tumor initiation and differentiation. H3K27ac profiles were analyzed to reveal 6 human SCLC specimen and 20 mice tumors epigenomic landscapes.

Measurements and Main Results: We identified an epigenomic subclusters of the major SCLC-A subtype, named SCLC-A1 and SCLC-A2. SCLC-A1 was characterized by the presence of a super-enhancer at the *NKX2-1* locus, which was observed in human SCLC specimens and a murine SCLC model. We found NKX2-1, a dual lung and neural lineage factor, is uniquely relevant in SCLC-A1. We further found maintenance of this neural identity in SCLC-A1 is mediated by collaborative transcriptional activity with another neuronal transcriptional factor SOX1.

Conclusions: We comprehensively describe an additional epigenomic heterogeneity of the major SCLC-A subtype, and define SCLC-A1 subtype by the core regulatory circuitry representing

NKX2-1 and SOX1 super-enhancers and their functional collaborations to maintain neuronal linage state. (Word count 250)

Keywords: small cell lung cancer (SCLC); *NKX2-1/TTF-1*; *SOX1*; Super-enhancer

95 **INTRODUCTION**

96 Small cell lung cancer (SCLC) is an aggressive, lethal, and rapidly progressing neuroendocrine
97 (NE) malignancy, accounting for ~15% of lung cancer incidence and 250,000 deaths worldwide
98 annually (1). The five-year survival rate for patients with SCLC is only 6% compared to 19% for
99 non-SCLC. The lack of progress in SCLC treatment is largely attributable to the inadequate
100 molecular understanding. Advances in genomic technology have enabled new molecular
101 characterization of SCLCs. Genome-wide methylation and transcriptomes of human SCLCs and
102 PDX models identified NE and non-NE subtypes. NE subtype is defined by the expression of
103 neuronal lineage transcription factors (TFs) ASCL1 and/or NeuroD1 (2). Two recent studies
104 described the non-NE SCLCs, one signified by YAP1 expression and another by POU2F3
105 expression (3, 4). In light of these findings, a consortium proposed a new molecular
106 classification of SCLCs that distinguishes them into four subtypes based on the expression of
107 four lineage-defining transcription factors: ASCL1, NeuroD1, YAP1 and POU2F3 referred to as
108 SCLC-A, SCLC-N, SCLC-Y and SCLC-P, respectively (5, 6). The classification, while marking
109 significant advance, is still a work in progress. After that report, a newer study proposed an
110 inflamed SCLC subtype (SCLC-I) (7). In addition, not all SCLCs clearly fall into the four
111 clusters as they often express multiple factors at variable levels, especially in the SCLC-A
112 subtype which account for 70% of SCLCs (8). This wide range of heterogeneity warrants novel
113 approaches to develop a more precise classification of SCLC based on lineage subtype.

114 Lineage-specific transcription factors and the presence of SE at their gene locus are
115 critical determinants of cellular identity (9). In our study, we applied epigenomic approaches to
116 investigate the differential enhancer landscapes in SCLC cell lines, human SCLC samples and
117 autochthonous murine SCLCs from a genetic engineered mouse model (GEMM) to reveal

118 additional intertumoral heterogeneity, providing comprehensive evidence of distinct histone
119 modification profiles. Furthermore, we determined a novel mechanism of subtype-specific
120 transcriptional regulation in SCLC, integrating the core transcriptional networks and their
121 collaborative regulation of NE target genes.

122 **METHODS**

123 For a detailed description of the methods, please see the online supplement.

124 ***Cell lines***

125 Cell lines used in this study are listed in Table E1.

126 ***Chromatin Immunoprecipitation followed by sequencing (ChIP-seq)***

127 ChIP-seq was performed as described previously (10). Protein G magnetic beads (Dynabeads:
128 Life Technologies) were pre-incubated with anti-H3K27ac (Abcam, ab4729) or anti-NKX2-1
129 (Bethyl Laboratories, A300-BL4000) or anti-SOX1 (R&D, AF3369) antibodies. Up to 10 ng of
130 DNA was used for the library construction using NEBNext Ultra II DNA Library Prep Kit (NEB,
131 E7645). Sequencing was performed on NextSeq 500 (Illumina).

132 ***RNA-seq***

133 The procedure was performed as previously described (8, 10).

134 ***Lentiviral transduction of genes and CRISPR-Cas9 genome editing***

135 *FLAG-NKX2-1* or *FLAG-GFP* open reading frame (ORF) was cloned into pLEX_306 (a gift
136 from David Root, Addgene plasmid #41391). Cells stably expressing Cas9 were generated by
137 infection with the lentiCas9-Blast plasmid (Addgene # 52962, a gift from Feng Zhang). sgRNAs
138 targeting *NKX2-1* or *SOX1* were selected from Brunello library (Table E2) (11). Additional
139 details are provided in the online supplement.

140 ***Immunohistochemistry (IHC)***

141 Immunohistochemical analyses were performed on xenograft tumor specimens, human primary
142 SCLC tumor specimens and genetic engineered mouse model (GEMM) tumor specimens with
143 anti-NKX2-1 (1:100; Santa Cruz, sc-53136), anti-SOX1 (R&D, AF3369) or anti-ASCL1 (1:100,
144 BD, 556604) antibody and detected with the Vectastain ABC kit.

145 ***Co-immunoprecipitation and LC-MS/MS***

146 Chromatin fraction was prepared and co-immunoprecipitated with the methods described
147 previously (12) with modifications. Peptides were detected, isolated, and fragmented to produce
148 a tandem mass-spectrum of specific fragment ions for each peptide with LTQ Orbitrap Velos Pro
149 ion-trap mass spectrometer (Thermo Fisher Scientific, Waltham, MA).

150 ***Cell proliferation assay***

151 Details are provided in the online supplement.

152 ***Xenograft model***

153 The procedure was performed as previously described (ref). All xenograft studies were approved
154 by the institutional Animal Care and Use Committee at Icahn School of Medicine at Mount Sinai
155 (IACUC-2018-0021).

156 ***Annexin-V staining***

157 Details are provided in the online supplement.

158 ***In situ proximity ligation assay (in situ PLA)***

159 *In situ* PLA was performed with DuoLink in Situ Reagents (Sigma) according to the instructions.
160 Images were acquired with a ZEISS Axiocam 503 mono confocal microscope.

161 ***Mice and tumor initiation***

162 Mice harboring $Rb1^{flox}$, $Trp53^{flox}$ and $Nkx2\text{-}1^{flox}$ alleles have been previously described (13, 14).
163 Tumors were generated by intratracheal delivery of Ad5CMV-Cre adenovirus (University of
164 Iowa, Gene Transfer Vector Core) as described (15). All studies were approved by the
165 Committee for Animal Care at MIT (A-3125–01).

166 ***Data analysis***

167 Details are provided in the online supplement.

168 ***Statistical Analysis***

169 Details of specific analyses are provided in the figure legends.

170 ***Data and materials availability***

171 SCLC cell lines, human primary SCLC tumors, RP and RPN tumors H3K27ac ChIP-seq, Cell
172 lines and RP and RPN tumors RNA-seq, NKX2-1 and SOX1 ChIP-seq are deposited in NCBI
173 GEO: GSE183373.

174 **RESULTS**

175 **Epigenomic profiling subdivided SCLC-A by differential super-enhancers**

176 Genome-scale chromatin organization of the cell more faithfully reflects their lineage state than
177 transcriptomics (16). To refine current SCLC classification, we profiled genome-wide H3K27ac
178 to define SE regions across 16 SCLC cell lines. Unsupervised hierarchical clustering on SEs on
179 genes for transcriptional regulation with additional public data (4) revealed four subclasses
180 (Figure 1A), supported by principal component analysis (PCA) (see Figure E1A in the online
181 data supplement). Our clusters recapitulated aspects of the expression classification. Cluster III
182 corresponds to SCLC-N (Figure 1A; purple). Cluster IV represents SCLC-P and SCLC-Y
183 (Figure 1A; blue). Notably, epigenomic clustering distinguished SCLC-A into two distinct
184 Clusters I and II (Figure 1A; red and green) referred to as SCLC-A1 and SCLC-A2, while
185 *ASCL1* SE is present in 92.9% (13/14) of SCLC-A (Figure E1B).

186 To understand the difference underpinning SCLC-A1 and SCLC-A2, we identified 140
187 differentially enriched SEs. Among 110 SEs enriched in SCLC-A1 was *NKX2-1* (Figure 1B),
188 where H3K27ac signal was largely absent in other subclasses (Figure 1C). The 30 SEs enriched
189 in SCLC-A2 included *TCF4*, a transcription factor that regulates synaptic plasticity (17) (Figure
190 1B and Figure E1B). NKX2-1, also known as *TTF1*, a lineage transcription factor essential for
191 the development and maintenance of lungs, brain, and thyroid, is a frequently amplified lineage-
192 specific oncogene and a well-known marker to diagnose lung adenocarcinoma (LADC) (18) (19,
193 20). However, *NKX2-1* is not significantly amplified in human SCLCs (21) nor in the SCLC
194 lines used (Figure E1C). Nonetheless, SCLC-A1 cell lines harbor *NKX2-1* SE, whereas SCLC-
195 A2 cell lines do not (Figure 1D and Figure E1D). Local H3K27ac enrichment pattern at the
196 *NKX2-1* locus in SCLC-A1 was almost identical to LADCs with *NKX2-1* amplification (Figure

197 E1E). In 6 human SCLC specimens, we found one SCLC-P tumor with *POU2F3* SE, and threes
198 mixed SCLC-A/N tumors with SEs near *ASCL1* and *NEUROD1* loci (Figure E1F). Notably, we
199 observed two tumors representing SCLC-A1 with high signals at *ASCL1* and *NKX2-1* loci
200 (Figure 1E).

201 By immunohistochemistry (IHC) on another 34 human SCLC cohort, 65% (22/34) of
202 cases were NKX2-1-positive (Figure E2A), consistent with prior studies (22-26). In cell lines,
203 SCLC-A1 expressed substantially higher levels of NKX2-1 protein than other SCLC subtypes
204 and equivalent to *NKX2-1*-amplified LADCs (Figure 1F). Furthermore, RNA-seq datasets (5, 27)
205 confirmed *NKX2-1* is highly expressed in SCLC (Figure E2B), particularly in SCLC-A (Figure
206 1G), comparable to the levels in LADC (Figure E2C), consistent with a previous report (22).
207 Nonetheless, non-bimodal distribution of *NKX2-1* expression suggests that the distinction
208 between SCLC-A1 and A2 is not discernible from expression analysis, perhaps analogous to the
209 findings that *NKX2-1* is almost universally expressed in LADC yet only amplified in 10-15%,
210 which we previously characterized as a distinct biological subgroup (19, 28).

211 ***NKX2-1* survival dependency is unique to SCLC-A1**

212 A recent study implicated that NKX2-1 promotes SCLC growth and regulates NE differentiation
213 and anti-apoptosis (29). We deleted *NKX2-1* in SCLC-A1 cell lines (Figure 2A) and found it
214 significantly suppressed cell growth and increased annexin-V-positive populations (Figure 2C
215 and E3A). By contrast, ablating NKX2-1 in SCLC cells from other clusters (Figure 2B) had little
216 effect. Given that acute removal of a master lineage factor in established cancer often leads to a
217 halt in cell growth (30), these data suggest NKX2-1 does not play a general oncogenic role in all
218 lineage states but its function is uniquely relevant to SCLC-A1.

219 We further found a significant decrease in tumor volume for NKX2-1-deleted SCLC-A1
220 cells in xenograft (Figure 2D and Figure E3B), confirming its essentiality *in vivo*. No obvious
221 histological differences were observed in the cells that formed small tumors which escaped from
222 NKX2-1 deletion (Figure E3C). In a short period after NKX2-1 deletion *in vitro*, expression of
223 NE markers was not significantly altered (Figure E3D). Overall, these data suggest that NKX2-1
224 is functionally critical for SCLC-A1 *in vitro* and *in vivo*.

225 **Genomic occupancy of *NKX2-1* in SCLC-A1 cells distinct from that in LADC cells**

226 In LADC, NKX2-1 regulates gene expression and shares its cistromes with normal lung
227 (19); however, SCLCs typically do not express canonical NKX2-1 targets. Given NKX2-1's
228 roles in subsets of cortical, striatal, and pallidal neurons (31), we speculated its potential role for
229 neuronal differentiation in SCLC-A1. Therefore, we profiled NKX2-1 cistromes by ChIP-seq in
230 5 SCLC-A1 cell lines and compared them to that from 3 LADC cell lines. Pairwise correlation
231 coefficient of all NKX2-1-bound sites and PCA revealed histology-specific binding profiles
232 (Figure 3A and E4A). Regions 4 (low-intensity signals) and 1 (high-intensity signals) are
233 common between SCLC-A1 and LADC (Figure 3B), which included the *RUNX1* locus (Figure
234 3C). Region 3 was unique to LADC that included *LMO3,* an essential mediator of NKX2-1
235 functions in LADCs (19). Region 2 was unique to SCLC-A1 that included *DCC,* a receptor for
236 netrin required for axon guidance (32) (Figure 3C). These data suggest NKX2-1 regulates
237 distinct transcriptional programs across these two lineage states.

238 Ontologies on 661 SCLC-A1-unique regions (Figure 3D and E4B) were enriched for
239 neuronal development, differentiation, and structure (Figure 3E). By contrast, genes regulating
240 neuronal biology were absent in LADC-unique regions (Figure E4C). Motif analysis revealed
241 SCLC-A1-specific sites are enriched with ASCL2, Olig2, and SOX motifs, suggesting more

242 association with neuronal TFs (Figure E4D). In contrast, AP-1, Ets, Runx, and Tead-binding
243 motifs are enriched in LADC-specific regions, consistent with our previous report (19). These
244 data indicate that contribution of NKX2-1 in regulating pathways for maintenance of neural
245 differentiation state of SCLC-A1, distinct from its role in normal lung epithelium and LADCs.

246 **NKX2-1 interactome in chromatin of SCLC-A1 cells includes SOX1**

247 NKX2-1 interacts with FOXA1 to co-regulate the expression of a set of genes for lineage control
248 in LADC (19, 20). Therefore, to identify unique partners that interact with NKX2-1 to exert
249 distinct transcriptional program in SCLC-A1, we performed co-immunoprecipitation (co-IP)
250 followed by liquid chromatography tandem mass-spectrometry (LC-MS/MS) in the chromatin
251 fraction of two SCLC-A1 cell lines ectopically expressing FLAG-NKX2-1 (Figure 4A and
252 Figure E5A). We found 27 overlapping NKX2-1-interacting TFs in both cell lines (Figure 4B).

253 We further identified core regulatory circuitries (CRCs) (33) for SCLC-A1 and other
254 SCLC clusters from our H3K27ac data. Common CRCs included NEUROD1 for SCLC-N,
255 POU2F3 and ASCL2 for SCLC-P/Y, and TCF4 in SCLC-A2, consistent with our differential SE
256 analysis (Figure 1B and E5B). Common CRCs in SCLC-A1 included NKX2-1 (Figure 4C) along
257 with SOX1, NFIB, TCF12 and PBX1 also found in the SCLC-A1 NKX2-1-interactome. Of those,
258 H3K27ac signal at *SOX1* was highly enriched in SCLC-A1 (Figure 1B and Figure 4D), whereas
259 *NFIB*, *TCF12* and *PBX1* SEs were present across SCLC subtypes (Figure E5C). *SOX1* is highly
260 expressed in SCLC-A (Figure E5D) and positively correlated with *NKX2-1* expression in 185
261 SCLC tumors and cell lines (Figure E5E). SOX1 protein was also highly expressed specifically
262 in SCLC-A1 cell lines (Figure E5F).

263 The interaction between NKX2-1 and SOX1 was confirmed by co-IP followed by
264 western blot in two SCLC-A1 cell lines (Figure 4E), and further by proximity ligation assay

265 (PLA) in 4 SCLC-A1 cell lines (Figure 4F and Figure E5G). These data suggest robust protein-
266 protein interaction between NKX2-1 and SOX1 uniquely in SCLC-A1.

267 **NKX2-1 and SOX1 co-occupy the SCLC-A1 genome to collaborate in neuronal gene**
268 **regulation**

269 Next, we profiled genome-wide binding profiles of NKX2-1 and SOX1 in four SCLC-A1 cell
270 lines and found the majority of SOX1 peaks were bound by NKX2-1 (48.6-67.8%) (Figure 5A).
271 The 2,652 regions co-bound by NKX2-1 and SOX1 in NCI-H187 were enriched for functions in
272 neuron differentiation and development, consistent with the aggregate analysis (Figure E6A and
273 E6B). We defined high-confidence NKX2-1 (5,663) and SOX1 (1,101) binding sites observed in
274 ≧3 cell lines, and found 604 peaks (54.9% of SOX1 peaks) are overlapped (Figure 5B), which
275 included the *NKX2-1* locus as well as neuronal genes *NRXN3* (34, 35) and *YWHAZ* (36) (Figure
276 5C) and ontologically enriched for functions in neuron differentiation and development (Figure
277 5D). These data suggest the interaction between NKX2-1 and SOX1 elicits specific cellular
278 identity of SCLC-A1.

279 **Collaboration of NKX2-1 and SOX1 is required to control the neuronal state in SCLC-A1**

280 We evaluated the transcriptional effect of depletion of *SOX1* or *NKX2-1* in NCI-H187 by RNA-
281 seq. After the abrogation of NKX2-1 or SOX1, 1,121 and 2,499 genes were significantly
282 downregulated respectively, with 873 genes commonly downregulated, suggesting a substantial
283 overlap in their transcriptional outputs (Figure 6A). We then queried the differentially co-
284 downregulated genes with the 2,652 genes with transcriptional start sites (TSSs) within 50 kb of
285 SOX1-NKX2-1 co-occupied peaks in NCI-H187, which were significantly enriched for NKX2-1
286 or SOX1 downregulated genes by ssGSEA analysis (Figure 6B). Leading edge analysis on these
287 genes revealed 289 overlaps, which we found are enriched for neuron differentiation and

288 development (Figure 6C). Together, these data suggest that NKX2-1 and SOX1 are specifically
289 co-localized on the SCLC-A1 genome and collaboratively contribute to controlling neuronal
290 differentiation state. We also found that SOX1 deletion, while not affecting the NKX2-1
291 expression, led to reduced cell growth (Figure E7A) with increased apoptosis (Figure E7B).

292 We previously found that expression of Nkx2-1 was critical for global Foxa1/2 binding
293 pattern in the LADC genome (20). To test if SOX1 is required for NKX2-1-binding to its target
294 genes in SCLC-A1, we performed NKX2-1 ChIP-seq in NCI-H187 cells upon SOX1 depletion.
295 Pairwise correlation coefficient of NKX2-1 peaks across cells deleted for SOX1 or control
296 revealed strong correlation amongst each group (Figure 6D), supported by PCA analysis (Figure
297 E7C). Differential analysis on NKX2-1-bound sites found 2,067 peaks decreased upon SOX1
298 deletion (Figure E7D). *k*-means clustering of the differential sites found relatively uniform
299 reduction of NKX2-1 binding after SOX1 deletion (Figure 6E), where we also found decreased
300 H3K27ac modification compared to other sites (Figure 6F), suggesting that these NKX2-1-lost
301 sites are no longer in active state, similar to a recent finding on Sox2 in esophageal squamous
302 cell cancer model for Klf5 (37). The data suggest that loss of SOX1 releases NKX2-1 from co-
303 occupied loci in SCLC-A1.

304 ***Nkx2-1* is essential for development of SCLC-A1 tumors in an autochthonous mouse model**

305 The *Rb1*$^{fl/fl}$*Trp53*$^{fl/fl}$ (RP) is commonly used SCLC models that recapitulates the biology of
306 ASCL1-positive/classic human SCLCs (13) (Figure 7A). We first profiled H3K27ac to identify
307 SEs in mSCLC tumors from RP model, where Nkx2-1 is diffusely expressed. We found all 10
308 tumors from 2 different mice harbored high-level H3K27ac signal around the *Ascl1* locus, but
309 none harbored SEs at the *Neurod1*, *Yap1* or *Pou2f3* locus, suggesting SCLC-A subtype (Figure
310 7B and Figure E8A) consistent with requirement of *Ascl1* for tumor formation in this model (38,

311 39). We found 3 of 10 tumors simultaneously had high-level H3K27ac signals at the *Nkx2-1* and
312 *Sox1* loci, reminiscent of SCLC-A1, while other 7 tumors have neither. This suggests that RP can
313 adopt an epigenetic state resembling either SCLC-A1 or SCLC-A2. Consistent but ambiguous
314 expression levels by IHC suggested epigenetic profiles distinguish these lineage classes more
315 clearly (Figure 7C).

316 To explore whether NKX2-1 contributes to mSCLC differentiation, we generated
317 *Rb1*$^{fl/fl}$*Trp53*$^{fl/fl}$*Nkx2-1*$^{fl/fl}$ (RPN) mice. We confirmed Nkx2-1 expression was absent in their
318 tumors, while 80% of them are Ascl1-positive suggesting that they remain representing SCLC-A.
319 Sox1 staining was only weakly positive in 6/10 cases while 4 other cases, including the two
320 Ascl1-negative tumors, were negative (Figure 7C). We observed no significant difference in
321 overall survival between the two genotypes (Figure E8B). Morphologically, all but one mSCLC
322 tumor from the RP model had classical SCLC morphology (scant cytoplasm, nuclei with fine
323 chromatin and inconspicuous nucleoli), whereas a subset of tumors in RPN mice (15% in RPN
324 vs. 4% in RP) exhibited a 'non-classical' histology defined by higher grade/vesicular nuclei by
325 two expert pathologists (E.L.S. and M.B) (Figure 7D). These suggest that loss of *Nkx2*-1 leads to
326 stochastic propensity to form non-classical morphology, the while majority of the tumors retain
327 classical histology representing SCLC-A.

328 Next, we profiled H3K27ac in 10 mSCLC tumors from four RPN mice (11-13 months
329 post-initiation, including five classical and five non-classical). None of the tumors from the RPN
330 mice had high-level H3K27ac signal at the *Neurod1*, *Yap1* or *Pou2f3* loci, whereas most of RPN
331 tumors (7/10) harbored high-level H3K27ac signals around the *Ascl1* locus (Figure 7B and
332 Figure E8A). Strikingly, we found signals at the *Nkx2-1* and the *Sox1* loci were absent in all RPN
333 tumors, suggesting SCLC-A2 subtype (Figure 7B). These data suggest that while the RP model

334 can develop both SCLC-A1 and SCLC-A2, *Nkx2-1* deletion at tumor initiation precludes SCLC-
335 A1 development.

336 Differential transcriptomic analysis from the tumors in RPN and RP mice also revealed
337 significantly downregulated genes in RPN tumors enriched for nervous system development
338 (Figure 7E), suggesting that SCLC-A2 is hierarchically closer to the SCLC-N and SCLC-Y/P
339 subtypes, also supported by the data that variant morphology is more frequent in RPN. To
340 address whether the absence of Nkx2-1 resulted in distinct tumor evolution in RPN, we profiled
341 copy numbers of those mSCLCs and found that *Nfib* and *Mycl* loci are frequently amplified in
342 RP model (6/10) consistent with previous reports; however, these amplifications were absent in
343 all tumors in RPN model, suggesting the lack of Nkx2-1 predisposed those RPN tumors to
344 undergo a distinct path leading to a different lineage class of tumors (Figure 7F and Figure E8C).

345 **DISCUSSION**

346 In the current classification, SCLC-A constitutes 70% of SCLCs, while emerging evidence
347 suggests its heterogeneity. Our study revealed distinctive epigenetic landscapes within SCLC-A
348 that we designated SCLC-A1 and SCLC-A2, characterized by the presence of *NKX2-1* and *TCF4*
349 SEs. NKX2-1 is required for the lung development and later specification of the peripheral lung,
350 but also of bronchial NE cells (40). NKX2-1 is a well-known marker to diagnose LADCs (41),
351 but it is also frequently expressed in SCLC. As NKX2-1 plays key roles in brain development
352 (42-45), it has been speculated that NKX2-1 is involved in NE pathways, based on its expression
353 enriched in SCLC-A (46) and its physical interaction with ASCL1 (29). In our study, while most
354 SCLC-A expresses NKX2-1 at variable levels, only 48% had *NKX2-1* SE. Importantly, *NKX2-1*
355 deletion in SCLC-A2 and SCLC-N cells, where NKX2-1 protein is still expressed, had little cell
356 growth effects, suggesting its relevancy only in SCLC-A1.

357 Further, our data suggest this function is mediated through interaction with SOX1.
358 Combinations of master TFs that assemble at tissue-specific cis-regulatory sites control distinct
359 cellular functions essential for maintaining lineage states in many contexts. Therefore, while the
360 role of SOX1 had never been described in the lung, it is plausible that their interaction is critical
361 to retain unique NE state and it further suggests biological plasticity between glandular cell
362 lineage and pulmonary NE lineage.

363 The roles of NKX2-1 in carcinogenesis are complex and remain poorly understood.
364 Nkx2-1 deletion in neoplastic lungs causes loss of pulmonary identity and reversion to a foregut
365 lineage. Our data suggest that Nkx2-1 contributes to maintaining a specific neural lineage state
366 that have classical SCLC morphology. The observation that *Nkx2-1* deletion is tolerated at tumor
367 initiation in the GEMM, but not in established human SCLC-A1 cell lines, provokes a few
368 potential interpretations. First, the timing of the deletion might be critical in determining the
369 outcome, as evidenced in other studies on lineage factors (47, 48). Second, as CMV-Cre targets
370 multiple cell types, *Nkx2-1* deletion may favor origination from certain cell types, thus
371 influencing tumor evolution, as reflected by the lack of amplification at *Nfib* and *Mycl*. Third,
372 early/in situ RPN lesions that would have become SCLC-A1 might simply evolve to an
373 alternative identity due to lack of *Nkx2-1*.

374 Together, we subdivided the major SCLC-A subtype into SCLC-A1 and SCLC-A2 by
375 revealing distinct epigenetic landscape in SCLC cell lines, human SCLC tumors, and GEMM.
376 Collaborative NKX2-1/SOX1 regulation defines the unique lineage state for SCLC-A1. This
377 study will provide foundation for future identification of vulnerabilities and enable us to develop
378 higher level of personalized therapeutic approaches to benefit SCLC patients.

Acknowledgements

We thank Hong Cai, Yi Ge, Ying Liu, Peipei Guo, Yifei Sun, Xiaokun Liu, Korey Kam, Mingzhe Li, Megan Vetter, Tyler Jacks and Karen Yee for helpful discussions and technical assistance, Aleksandra Wroblewska and Brian D. Brown for providing a lentiviral vector for cloning sgRNAs; NextSeq Sequencing Facility of the Department of Oncological Sciences at Icahn School of Medicine at Mount Sinai (ISMMS), Saboor Hekmaty, Gayatri Panda and Ravi Sachidanandam for sequencing assistance. The authors thank Taplin Mass Spectrometry Facility at Harvard Medical School, the Biorepository and Pathology Core Facility and Center for Comparative Medicine and Surgery at ISMMS.

388 **References**

389 1. Siegel RL, Miller KD, Jemal A. Cancer statistics, 2019. *CA Cancer J Clin* 2019; 69: 7-34.
390 2. Poirier JT, Gardner EE, Connis N, Moreira AL, de Stanchina E, Hann CL, Rudin CM. DNA methylation in
391 small cell lung cancer defines distinct disease subtypes and correlates with high expression of
392 EZH2. *Oncogene* 2015; 34: 5869-5878.
393 3. McColl K, Wildey G, Sakre N, Lipka MB, Behtaj M, Kresak A, Chen Y, Yang M, Velcheti V, Fu P, Dowlati
394 A. Reciprocal expression of INSM1 and YAP1 defines subgroups in small cell lung cancer.
395 *Oncotarget* 2017; 8: 73745-73756.
396 4. Huang YH, Klingbeil O, He XY, Wu XLS, Arun G, Lu B, Somerville TDD, Milazzo JP, Wilkinson JE,
397 Demerdash OE, Spector DL, Egeblad M, Shi JW, Vakoc CR. POU2F3 is a master regulator of a tuft
398 cell-like variant of small cell lung cancer. *Gene Dev* 2018; 32: 915-928.
399 5. George J, Lim JS, Jang SJ, Cun Y, Ozretic L, Kong G, Leenders F, Lu X, Fernandez-Cuesta L, Bosco G,
400 Muller C, Dahmen I, Jahchan NS, Park KS, Yang D, Karnezis AN, Vaka D, Torres A, Wang MS,
401 Korbel JO, Menon R, Chun SM, Kim D, Wilkerson M, Hayes N, Engelmann D, Putzer B, Bos M,
402 Michels S, Vlasic I, Seidel D, Pinther B, Schaub P, Becker C, Altmuller J, Yokota J, Kohno T,
403 Iwakawa R, Tsuta K, Noguchi M, Muley T, Hoffmann H, Schnabel PA, Petersen I, Chen Y,
404 Soltermann A, Tischler V, Choi CM, Kim YH, Massion PP, Zou Y, Jovanovic D, Kontic M, Wright
405 GM, Russell PA, Solomon B, Koch I, Lindner M, Muscarella LA, la Torre A, Field JK, Jakopovic M,
406 Knezevic J, Castanos-Velez E, Roz L, Pastorino U, Brustugun OT, Lund-Iversen M, Thunnissen E,
407 Kohler J, Schuler M, Botling J, Sandelin M, Sanchez-Cespedes M, Salvesen HB, Achter V, Lang U,
408 Bogus M, Schneider PM, Zander T, Ansen S, Hallek M, Wolf J, Vingron M, Yatabe Y, Travis WD,
409 Nurnberg P, Reinhardt C, Perner S, Heukamp L, Buttner R, Haas SA, Brambilla E, Peifer M, Sage J,
410 Thomas RK. Comprehensive genomic profiles of small cell lung cancer. *Nature* 2015; 524: 47-53.
411 6. Rudin CM, Poirier JT, Byers LA, Dive C, Dowlati A, George J, Heymach JV, Johnson JE, Lehman JM,
412 MacPherson D, Massion PP, Minna JD, Oliver TG, Quaranta V, Sage J, Thomas RK, Vakoc CR,
413 Gazdar AF. Molecular subtypes of small cell lung cancer: a synthesis of human and mouse model
414 data. *Nat Rev Cancer* 2019; 19: 289-297.
415 7. Gay CM, Stewart CA, Park EM, Diao L, Groves SM, Heeke S, Nabet BY, Fujimoto J, Solis LM, Lu W, Xi Y,
416 Cardnell RJ, Wang Q, Fabbri G, Cargill KR, Vokes NI, Ramkumar K, Zhang B, Della Corte CM,
417 Robson P, Swisher SG, Roth JA, Glisson BS, Shames DS, Wistuba, II, Wang J, Quaranta V, Minna J,
418 Heymach JV, Byers LA. Patterns of transcription factor programs and immune pathway
419 activation define four major subtypes of SCLC with distinct therapeutic vulnerabilities. *Cancer*
420 *Cell* 2021; 39: 346-360 e347.
421 8. Patel AS, Yoo S, Kong R, Sato T, Sinha A, Karam S, Bao L, Fridrikh M, Emoto K, Nudelman G, Powell CA,
422 Beasley MB, Zhu J, Watanabe H. Prototypical oncogene family Myc defines unappreciated
423 distinct lineage states of small cell lung cancer. *Sci Adv* 2021; 7.
424 9. Iwafuchi-Doi M, Zaret KS. Pioneer transcription factors in cell reprogramming. *Genes Dev* 2014; 28:
425 2679-2692.
426 10. Sato T, Yoo S, Kong R, Sinha A, Chandramani-Shivalingappa P, Patel A, Fridrikh M, Nagano O, Masuko
427 T, Beasley MB, Powell CA, Zhu J, Watanabe H. Epigenomic profiling discovers trans-lineage SOX2
428 partnerships driving tumor heterogeneity in lung squamous cell carcinoma. *Cancer Res* 2019.
429 11. Doench JG, Fusi N, Sullender M, Hegde M, Vaimberg EW, Donovan KF, Smith I, Tothova Z, Wilen C,
430 Orchard R, Virgin HW, Listgarten J, Root DE. Optimized sgRNA design to maximize activity and
431 minimize off-target effects of CRISPR-Cas9. *Nat Biotechnol* 2016; 34: 184-191.
432 12. Watanabe H, Ma Q, Peng S, Adelmant G, Swain D, Song W, Fox C, Francis JM, Pedamallu CS, DeLuca
433 DS, Brooks AN, Wang S, Que J, Rustgi AK, Wong KK, Ligon KL, Liu XS, Marto JA, Meyerson M, Bass

434 AJ. SOX2 and p63 colocalize at genetic loci in squamous cell carcinomas. *J Clin Invest* 2014; 124:
435 1636-1645.
436 13. Meuwissen R, Linn SC, Linnoila RI, Zevenhoven J, Mooi WJ, Berns A. Induction of small cell lung
437 cancer by somatic inactivation of both Trp53 and Rb1 in a conditional mouse model. *Cancer Cell*
438 2003; 4: 181-189.
439 14. Kusakabe T, Kawaguchi A, Hoshi N, Kawaguchi R, Hoshi S, Kimura S. Thyroid-specific enhancer-
440 binding protein/NKX2.1 is required for the maintenance of ordered architecture and function of
441 the differentiated thyroid. *Mol Endocrinol* 2006; 20: 1796-1809.
442 15. DuPage M, Dooley AL, Jacks T. Conditional mouse lung cancer models using adenoviral or lentiviral
443 delivery of Cre recombinase. *Nature protocols* 2009; 4: 1064-1072.
444 16. Zheng H, Xie W. The role of 3D genome organization in development and cell differentiation. *Nat Rev*
445 *Mol Cell Biol* 2019; 20: 535-550.
446 17. Kennedy AJ, Rahn EJ, Paulukaitis BS, Savell KE, Kordasiewicz HB, Wang J, Lewis JW, Posey J, Strange
447 SK, Guzman-Karlsson MC, Phillips SE, Decker K, Motley ST, Swayze EE, Ecker DJ, Michael TP, Day
448 JJ, Sweatt JD. Tcf4 Regulates Synaptic Plasticity, DNA Methylation, and Memory Function. *Cell*
449 *Rep* 2016; 16: 2666-2685.
450 18. Campbell JD, Alexandrov A, Kim J, Wala J, Berger AH, Pedamallu CS, Shukla SA, Guo G, Brooks AN,
451 Murray BA, Imielinski M, Hu X, Ling S, Akbani R, Rosenberg M, Cibulskis C, Ramachandran A,
452 Collisson EA, Kwiatkowski DJ, Lawrence MS, Weinstein JN, Verhaak RG, Wu CJ, Hammerman PS,
453 Cherniack AD, Getz G, Cancer Genome Atlas Research N, Artyomov MN, Schreiber R, Govindan R,
454 Meyerson M. Distinct patterns of somatic genome alterations in lung adenocarcinomas and
455 squamous cell carcinomas. *Nat Genet* 2016; 48: 607-616.
456 19. Watanabe H, Francis JM, Woo MS, Etemad B, Lin W, Fries DF, Peng S, Snyder EL, Tata PR, Izzo F,
457 Schinzel AC, Cho J, Hammerman PS, Verhaak RG, Hahn WC, Rajagopal J, Jacks T, Meyerson M.
458 Integrated cistromic and expression analysis of amplified NKX2-1 in lung adenocarcinoma
459 identifies LMO3 as a functional transcriptional target. *Genes Dev* 2013; 27: 197-210.
460 20. Snyder EL, Watanabe H, Magendantz M, Hoersch S, Chen TA, Wang DG, Crowley D, Whittaker CA,
461 Meyerson M, Kimura S, Jacks T. Nkx2-1 represses a latent gastric differentiation program in lung
462 adenocarcinoma. *Mol Cell* 2013; 50: 185-199.
463 21. Peifer M, Fernandez-Cuesta L, Sos ML, George J, Seidel D, Kasper LH, Plenker D, Leenders F, Sun R,
464 Zander T, Menon R, Koker M, Dahmen I, Muller C, Di Cerbo V, Schildhaus HU, Altmuller J,
465 Baessmann I, Becker C, de Wilde B, Vandesompele J, Bohm D, Ansen S, Gabler F, Wilkening I,
466 Heynck S, Heuckmann JM, Lu X, Carter SL, Cibulskis K, Banerji S, Getz G, Park KS, Rauh D, Grutter
467 C, Fischer M, Pasqualucci L, Wright G, Wainer Z, Russell P, Petersen I, Chen Y, Stoelben E, Ludwig
468 C, Schnabel P, Hoffmann H, Muley T, Brockmann M, Engel-Riedel W, Muscarella LA, Fazio VM,
469 Groen H, Timens W, Sietsma H, Thunnissen E, Smit E, Heideman DA, Snijders PJ, Cappuzzo F,
470 Ligorio C, Damiani S, Field J, Solberg S, Brustugun OT, Lund-Iversen M, Sanger J, Clement JH,
471 Soltermann A, Moch H, Weder W, Solomon B, Soria JC, Validire P, Besse B, Brambilla E, Brambilla
472 C, Lantuejoul S, Lorimier P, Schneider PM, Hallek M, Pao W, Meyerson M, Sage J, Shendure J,
473 Schneider R, Buttner R, Wolf J, Nurnberg P, Perner S, Heukamp LC, Brindle PK, Haas S, Thomas
474 RK. Integrative genome analyses identify key somatic driver mutations of small-cell lung cancer.
475 *Nat Genet* 2012; 44: 1104-1110.
476 22. Horie M, Miyashita N, Mattsson JSM, Mikami Y, Sandelin M, Brunnstrom H, Micke P, Nagase T, Saito
477 A. An integrative transcriptome analysis reveals a functional role for thyroid transcription factor-
478 1 in small cell lung cancer. *J Pathol* 2018; 246: 154-165.
479 23. Misch D, Blum T, Boch C, Weiss T, Crolow C, Griff S, Mairinger T, Bauer TT, Kollmeier J. Value of
480 thyroid transcription factor (TTF)-1 for diagnosis and prognosis of patients with locally advanced
481 or metastatic small cell lung cancer. *Diagn Pathol* 2015; 10: 21.

482 24. Miyauchi E, Motoi N, Ono H, Ninomiya H, Ohyanagi F, Nishio M, Okumura S, Ichinose M, Ishikawa Y.
483 Distinct Characteristics of Small Cell Lung Cancer Correlate With Central or Peripheral Origin:
484 Subtyping Based on Location and Expression of Transcription Factor TTF-1. *Medicine (Baltimore)*
485 2015; 94: e2324.
486 25. Wu M, Wang B, Gil J, Sabo E, Miller L, Gan L, Burstein DE. p63 and TTF-1 immunostaining. A useful
487 marker panel for distinguishing small cell carcinoma of lung from poorly differentiated
488 squamous cell carcinoma of lung. *Am J Clin Pathol* 2003; 119: 696-702.
489 26. Ordonez NG. Value of thyroid transcription factor-1 immunostaining in distinguishing small cell lung
490 carcinomas from other small cell carcinomas. *Am J Surg Pathol* 2000; 24: 1217-1223.
491 27. Jiang L, Huang J, Higgs BW, Hu Z, Xiao Z, Yao X, Conley S, Zhong H, Liu Z, Brohawn P, Shen D, Wu S,
492 Ge X, Jiang Y, Zhao Y, Lou Y, Morehouse C, Zhu W, Sebastian Y, Czapiga M, Oganesyan V, Fu H,
493 Niu Y, Zhang W, Streicher K, Tice D, Zhao H, Zhu M, Xu L, Herbst R, Su X, Gu Y, Li S, Huang L, Gu J,
494 Han B, Jallal B, Shen H, Yao Y. Genomic Landscape Survey Identifies SRSF1 as a Key Oncodriver in
495 Small Cell Lung Cancer. *PLoS Genet* 2016; 12: e1005895.
496 28. Weir BA, Woo MS, Getz G, Perner S, Ding L, Beroukhim R, Lin WM, Province MA, Kraja A, Johnson LA,
497 Shah K, Sato M, Thomas RK, Barletta JA, Borecki IB, Broderick S, Chang AC, Chiang DY, Chirieac
498 LR, Cho J, Fujii Y, Gazdar AF, Giordano T, Greulich H, Hanna M, Johnson BE, Kris MG, Lash A, Lin L,
499 Lindeman N, Mardis ER, McPherson JD, Minna JD, Morgan MB, Nadel M, Orringer MB, Osborne
500 JR, Ozenberger B, Ramos AH, Robinson J, Roth JA, Rusch V, Sasaki H, Shepherd F, Sougnez C,
501 Spitz MR, Tsao MS, Twomey D, Verhaak RG, Weinstock GM, Wheeler DA, Winckler W, Yoshizawa
502 A, Yu S, Zakowski MF, Zhang Q, Beer DG, Wistuba, II, Watson MA, Garraway LA, Ladanyi M,
503 Travis WD, Pao W, Rubin MA, Gabriel SB, Gibbs RA, Varmus HE, Wilson RK, Lander ES, Meyerson
504 M. Characterizing the cancer genome in lung adenocarcinoma. *Nature* 2007; 450: 893-898.
505 29. Hokari S, Tamura Y, Kaneda A, Katsura A, Morikawa M, Murai F, Ehata S, Tsutsumi S, Ishikawa Y,
506 Aburatani H, Kikuchi T, Miyazono K, Koinuma D. Comparative analysis of TTF-1-binding DNA
507 regions in small cell lung cancer and non-small cell lung cancer. *Mol Oncol* 2019.
508 30. Heinz S, Romanoski CE, Benner C, Glass CK. The selection and function of cell type-specific enhancers.
509 *Nat Rev Mol Cell Biol* 2015; 16: 144-154.
510 31. Magno L, Barry C, Schmidt-Hieber C, Theodotou P, Hausser M, Kessaris N. NKX2-1 Is Required in the
511 Embryonic Septum for Cholinergic System Development, Learning, and Memory. *Cell Rep* 2017;
512 20: 1572-1584.
513 32. Liu Y, Bhowmick T, Liu Y, Gao X, Mertens HDT, Svergun DI, Xiao J, Zhang Y, Wang JH, Meijers R.
514 Structural Basis for Draxin-Modulated Axon Guidance and Fasciculation by Netrin-1 through DCC.
515 *Neuron* 2018; 97: 1261-1267 e1264.
516 33. Saint-Andre V, Federation AJ, Lin CY, Abraham BJ, Reddy J, Lee TI, Bradner JE, Young RA. Models of
517 human core transcriptional regulatory circuitries. *Genome Res* 2016; 26: 385-396.
518 34. Reissner C, Runkel F, Missler M. Neurexins. *Genome Biol* 2013; 14: 213.
519 35. Sudhof TC. Neuroligins and neurexins link synaptic function to cognitive disease. *Nature* 2008; 455:
520 903-911.
521 36. Toma C, Torrico B, Hervas A, Valdes-Mas R, Tristan-Noguero A, Padillo V, Maristany M, Salgado M,
522 Arenas C, Puente XS, Bayes M, Cormand B. Exome sequencing in multiplex autism families
523 suggests a major role for heterozygous truncating mutations. *Mol Psychiatry* 2014; 19: 784-790.
524 37. Wu Z, Zhou J, Zhang X, Zhang Z, Xie Y, Liu JB, Ho ZV, Panda A, Qiu X, Cejas P, Canadas I, Akarca FG,
525 McFarland JM, Nagaraja AK, Goss LB, Kesten N, Si L, Lim K, Liu Y, Zhang Y, Baek JY, Liu Y, Patil DT,
526 Katz JP, Hai J, Bao C, Stachler M, Qi J, Ishizuka JJ, Nakagawa H, Rustgi AK, Wong KK, Meyerson M,
527 Barbie DA, Brown M, Long H, Bass AJ. Reprogramming of the esophageal squamous carcinoma
528 epigenome by SOX2 promotes ADAR1 dependence. *Nat Genet* 2021; 53: 881-894.

529 38. Borromeo MD, Savage TK, Kollipara RK, He M, Augustyn A, Osborne JK, Girard L, Minna JD, Gazdar AF,
530 Cobb MH, Johnson JE. ASCL1 and NEUROD1 Reveal Heterogeneity in Pulmonary Neuroendocrine
531 Tumors and Regulate Distinct Genetic Programs. *Cell Rep* 2016; 16: 1259-1272.
532 39. Olsen RR, Ireland AS, Kastner DW, Groves SM, Spainhower KB, Pozo K, Kelenis DP, Whitney CP,
533 Guthrie MR, Wait SJ, Soltero D, Witt BL, Quaranta V, Johnson JE, Oliver TG. ASCL1 represses a
534 SOX9(+) neural crest stem-like state in small cell lung cancer. *Genes Dev* 2021; 35: 847-869.
535 40. La Rosa S, Chiaravalli AM, Placidi C, Papanikolaou N, Cerati M, Capella C. TTF1 expression in normal
536 lung neuroendocrine cells and related tumors: immunohistochemical study comparing two
537 different monoclonal antibodies. *Virchows Arch* 2010; 457: 497-507.
538 41. Yamaguchi T, Hosono Y, Yanagisawa K, Takahashi T. NKX2-1/TTF-1: an enigmatic oncogene that
539 functions as a double-edged sword for cancer cell survival and progression. *Cancer Cell* 2013; 23:
540 718-723.
541 42. Puelles L, Kuwana E, Puelles E, Bulfone A, Shimamura K, Keleher J, Smiga S, Rubenstein JL. Pallial and
542 subpallial derivatives in the embryonic chick and mouse telencephalon, traced by the expression
543 of the genes Dlx-2, Emx-1, Nkx-2.1, Pax-6, and Tbr-1. *J Comp Neurol* 2000; 424: 409-438.
544 43. Flames N, Pla R, Gelman DM, Rubenstein JL, Puelles L, Marin O. Delineation of multiple subpallial
545 progenitor domains by the combinatorial expression of transcriptional codes. *J Neurosci* 2007;
546 27: 9682-9695.
547 44. Sussel L, Marin O, Kimura S, Rubenstein JL. Loss of Nkx2.1 homeobox gene function results in a
548 ventral to dorsal molecular respecification within the basal telencephalon: evidence for a
549 transformation of the pallidum into the striatum. *Development* 1999; 126: 3359-3370.
550 45. Minocha S, Valloton D, Ypsilanti AR, Fiumelli H, Allen EA, Yanagawa Y, Marin O, Chedotal A, Hornung
551 JP, Lebrand C. Nkx2.1-derived astrocytes and neurons together with Slit2 are indispensable for
552 anterior commissure formation. *Nat Commun* 2015; 6: 6887.
553 46. Cardnell RJ, Li L, Sen T, Bara R, Tong P, Fujimoto J, Ireland AS, Guthrie MR, Bheddah S, Banerjee U,
554 Kalu NN, Fan YH, Dylla SJ, Johnson FM, Wistuba, II, Oliver TG, Heymach JV, Glisson BS, Wang J,
555 Byers LA. Protein expression of TTF1 and cMYC define distinct molecular subgroups of small cell
556 lung cancer with unique vulnerabilities to aurora kinase inhibition, DLL3 targeting, and other
557 targeted therapies. *Oncotarget* 2017; 8: 73419-73432.
558 47. Camolotto SA, Pattabiraman S, Mosbruger TL, Jones A, Belova VK, Orstad G, Streiff M, Salmond L,
559 Stubben C, Kaestner KH, Snyder EL. FoxA1 and FoxA2 drive gastric differentiation and suppress
560 squamous identity in NKX2-1-negative lung cancer. *Elife* 2018; 7.
561 48. Zewdu R, Mehrabad EM, Ingram K, Fang P, Gillis KL, Camolotto SA, Orstad G, Jones A, Mendoza MC,
562 Spike BT, Snyder EL. An NKX2-1/ERK/WNT feedback loop modulates gastric identity and
563 response to targeted therapy in lung adenocarcinoma. *Elife* 2021; 10.

564

565 **Figure legends**

566 **Figure 1. Epigenomic profiling subdivided SCLC-A by differential super-enhancers**

567 (**A**). Unsupervised hierarchical clustering of 25 SCLC cell lines using SE signals near
568 transcriptional regulator genes. The color scale indicates the intensity of SE signals normalized
569 to linear scores using the sum of squares of the values. Each row represents a SE locus (747 loci).
570 The color shades on the dendrogram indicate four novel SE clusters, the top red columns display
571 the presence of SE near the *NKX2-1* locus, and the bottom column colors denote the consensus
572 expression clusters. (**B**). Volcano plot showing 140 differentially enriched SEs (110 enriched in
573 SCLC-A1 and 30 enriched in SCLC-A2) at thresholds of absolute fold change ≥ 5 and FDR ≤
574 0.25 depicted as dotted lines. (**C**). Genome view tracks of H3K27ac signal at the *NKX2-1* locus
575 in four clusters of SCLC cell lines. Normalized scales are shown in Figure E1B. (**D**). SE plots
576 with all enhancers rank-ordered by H3K27ac signals in DMS 79, NCI-H187, NCI-H209 and
577 NCI-H345. Dotted lines depict tangential cutoffs to define SEs. (**E**). Genome view tracks of
578 H3K27ac signals at the *ASCL1*, *NEUROD1*, *POU2F3*, *YAP1* and *NKX2-1* loci in 2 human SCLC
579 specimens of SCLC-A subtype. (**F**). Protein expression of NKX2-1, ASCL1 and vinculin as a
580 loading control in SCLC cell lines from different clusters. *NKX2-1*-amplified adenocarcinoma
581 cell lines NCI-H3122 and NCI-H2087 are shown as reference. (**G**). Box and jitter plots showing
582 the distribution of *NKX2-1* mRNA expression in SCLC-A, SCLC-N, SCLC-P, and SCLC-Y
583 subtypes of 135 primary SCLC tumors.

584 **Figure 2. *NKX2-1* survival dependency is unique to SCLC-A1**

585 (**A**). *(Top)* Immunoblots showing protein expression of NKX2-1 and vinculin as a loading
586 control in SCLC-A1 cell lines with three *NKX2-1* sgRNAs, or two non-target (NT) sgRNAs.

587 *(Bottom)* Cell growth curve for SCLC-A1 cell lines infected with *NKX2-1* sgRNAs or NT
588 sgRNAs. Data are shown as mean ± SD (n=3); *P < 0.0001 by two-sided two-way ANOVA. (**B**).
589 *(Top)* Immunoblots showing protein expression of NKX2-1 and vinculin as a loading control in
590 SCLC-A2 (NCI-H2171, NCI-H69) and SCLC-N (NCI-H1963) cell lines with *NKX2-1* sgRNAs,
591 or non-target (NT) sgRNAs. *(Bottom)* Cell growth curve for cell lines infected with *NKX2-1*
592 sgRNA or NT sgRNAs. Data are shown as mean ± SD (n=3); *P < 0.0001 by two-sided two-way
593 ANOVA. (**C**). Bar plots showing percentage of apoptotic NCI-H187 cells infected with NT
594 sgRNA and *NKX2-1* sgRNA, measured by annexin V staining. Means ± SD of three biological
595 replicates. *P < 0.0001, t test. Representative data for NT sg1 and NKX2-1 sg1 can be found in
596 Figure E2A. (**D**). (*Left*) Tumor growth curve for xenograft tumors of NCI-H187 cells infected
597 with *NKX2-1* sg1 or NT sg1 *in vivo*. Mean ± SD of four biological replicates. *P < 0.0001, t test.
598 Xenograft tumors were resected at 3 weeks after inoculation. (*Right*) Images of resected
599 xenograft tumors of NCI-H209 cells infected with NT sg1 or *NKX2-1* sg1 *in vivo* at day 23.

600 **Figure 3. Genomic occupancy of *NKX2-1* in SCLC-A1 cells distinct from that in LADC**
601 **cells**

602 (**A**). Correlation matrix depicting pairwise comparisons of identified NKX2-1 binding peaks in
603 the 5 SCLC-A1 cell lines and in 3 LADC cell lines. Color scale represents degree of Pearson's
604 correlation coefficient. (**B**). Heatmap showing signals from NKX2-1 ChIP-seq data in the 5
605 SCLC-A1 cell lines and 3 LUAC cell lines. ChIP signal intensity is shown by red shading. Y-
606 axis contains all peaks that are bound by NKX2-1 in any of SCLC-A1 and LUAC (n=37,198).
607 Peaks are divided into 4 regions by *k-means* (k=4) clustering. (**C**). NKX2-1 ChIP-seq signals in
608 SCLC-A1 and LADC cell lines at representative loci (*RUNX1*; cluster 1, *LMO3*; cluster 3 and
609 *DCC*; cluster 2). Red: SCLC-A1 cell lines. Black: LADC cell lines. (**D**). Heatmap showing 2,671

610 differentially NKX2-1 bound regions (fold change ≥ 2^5 and FDR ≤ $1x10^{-5}$), 2,010 enriched in
611 LADC and 661 enriched in SCLC-A1, between 5 SCLC-A1 cell lines and 3 LUAC cell lines. (**E**).
612 Enriched ontology by GREAT analyses for regions differentially bound by NKX2-1 in 5 SCLC-
613 A1 compared to LADCs.

614 **Figure 4. NKX2-1 interactome in chromatin of SCLC-A1 cells includes SOX1**

615 (**A**). Experimental strategy to identify binding partners of NKX2-1 in SCLC-A1. Chromatin
616 prepared from the nuclear fraction of SCLC-A1 cell lines NCI-H187 and NCI-H1436 stably
617 expressing FLAG-NKX2-1 was solubilized using micrococcal nuclease digestion. Co-
618 immunoprecipitated proteins with anti-FLAG antibody from solubilized chromatin were
619 identified by LC-MS/MS (see Data file S2 for the complete list). (**B**). Venn diagram showing the
620 number of transcription factors identified in each of the 2 SCLC-A1 cell lines and the 27
621 overlaps found in both cell lines. The proteins indicated in yellow color were also found in CRC
622 analysis in Figure 4C. (**C**). Core transcriptional regulatory circuitries (CRCs) commonly
623 identified in 8 SCLC-A1 cell lines. The genes in yellow color were also found in LC-MS/MS
624 analysis in Figure 4B. (**D**). Genome view tracks of H3K27ac signal at the *SOX1* locus in four
625 clusters of SCLC cell lines. (**E**). Immunoblots with anti-SOX1 antibody on endogenous co-
626 immunoprecipitates by anti-NKX2-1 antibody in SCLC-A1 (DMS 79 and NCI-H187) cells. (**F**).
627 *In situ* proximity ligation assay signals (red fluorescence) targeting endogenous SOX1 and
628 NKX2-1 in NCI-H841, NCI-H187, NCI-H209 and DMS 79 cells. Nuclei are counterstained with
629 DAPI (blue). See Figure E4G for additional control.

630 **Figure 5. NKX2-1 and SOX1 co-occupy the SCLC-A1 genome to collaborate in gene**
631 **regulation**

632 (**A**). Heatmap showing k-means clustering (*k*=4) of signals at the common 4,051 loci from
633 NKX2-1 (red) and SOX1 (blue) ChIP-seq data in the 4 SCLC-A1 cell lines. ChIP signal intensity
634 is shown by shading for all NKX2-1 and SOX1 occupied loci. (**B**). Venn diagram showing the
635 overlap of NKX2-1 common binding sites and SOX1 common binding sites present in at least 3
636 SCLC-A1 cell lines. (**C**). Genome view tracks of NKX2-1 (red) and SOX1 (blue) ChIP-seq
637 signals in four SCLC-A1 (DMS 79, NCI-H187, NCI-H209 and NCI-H345) cell lines and 3
638 LADC cell lines at the representative NKX2-1-SOX1 co-occupied loci (*NRXN3* and *YWHAZ*;
639 SCLC-A1 unique, *NKX2-1*; SCLC-A1/LADC common). (**D**). Enriched ontology by GREAT
640 analyses for regions in 604 overlapping high-confidence NKX2-1-SOX1 binding sites.

641 **Figure 6. Collaboration of NKX2-1 and SOX1 is required to control the neuronal state in**
642 **SCLC-A1**

643 (**A**). Venn diagram showing the overlap of downregulated genes after depletion of NKX2-1 (fold
644 change > 1.4 and adjusted P < 0.05) and SOX1 (fold change > 2 and adjusted P < 0.05) in NCI-
645 H187 cells. (**B**). Gene Set Enrichment Analysis (GSEA) of genes associated with 2,652 NKX2-
646 1-SOX1 co-occupied loci for expression data upon repression of NKX2-1 (*left*) or SOX1 (*right*)
647 in NCI-H187 cells, with their leading-edge genes shaded. Enrichment was significant for both
648 (NES= -2.29, P < 0.001 for NKX2-1 and NES= -2.54, P < 0.001 for SOX1). (**C**). Enriched gene
649 ontologies (MSigDB, biological process) for 289 common genes in leading-edge genes for both
650 NKX2-1 and SOX1 deletions. (**D**). Correlation matrix depicting pairwise comparisons of
651 identified NKX2-1 binding regions in three *SOX1* sgRNAs and three control cells (two non-
652 target (NT) sgRNAs, one parental cell) of NCI-H187 cell line. Color scale represents degree of
653 Pearson's correlation coefficient. (**E**). Heatmap showing k-means clustering (*k*=4) of 2,067
654 NKX2-1 ChIP-seq loci in NCI-H187 sgSOX1 compared to control cells with reduced signal

655 intensity. ChIP-seq signal intensity is shown by color shading. (**F**). Average H3K27ac ChIP-seq
656 signals on NKX2-1 reduced binding sites and NKX2-1 non-reduced binding sites defined in
657 Figure E6D for NCI-H187 parental, NT sg1, SOX1 sg2 and SOX1 sg3 cells.

658 **Figure 7. *Nkx2-1* is essential for development of SCLC-A1 tumors in an autochthonous**
659 **mouse model**

660 (**A**). Genetically engineered mouse models of SCLCs. *Rb1*$^{flox/flox}$; *Trp53*$^{flox/flox}$ (RP) mice or
661 *Rb1*$^{flox/flox}$; *Trp53*$^{flox/flox}$, *Nkx2-1* $^{flox/flox}$ (RPN) mice were transduced with Adeno-CMV-*Cre* to
662 initiate SCLC. (**B**). Genome view tracks at the Nkx2-1, Sox1, and Ascl1 loci for H3K27ac ChIP-
663 seq signals in 10 SCLC tumors from RP mice and 10 SCLC tumors from RPN mice. * indicates
664 3 tumors that have high-level signal at both *Nkx2-1* and *Sox1* loci. The arrowheads on *Nkx2-*
665 *1* locus indicate the loxP sites in RPN mice**.** (**C**). Representative immune-staining images for
666 Nkx2-1, Sox1, and Ascl1 on SCLC tumors from RP and RPN mice. Scale bars, 25µm. (**D**).
667 Representative hematoxylin and eosin (H&E) images of SCLC tumors from RP and RPN mice.
668 Scale bars, 2.5mm and 50µm, respectively. (**E**). Enriched gene ontologies (MSigDB, biological
669 process) for the differentially downregulated genes in RPN tumors compared to RP tumors. (**F**).
670 Average copy number profiles in RP and RPN models. Arrows indicate the *Nfib* and *Mycl* loci
671 that are specifically amplified in RP tumors (individual copy number profiles at those loci are
672 available in Figure E8C).

Figure 1

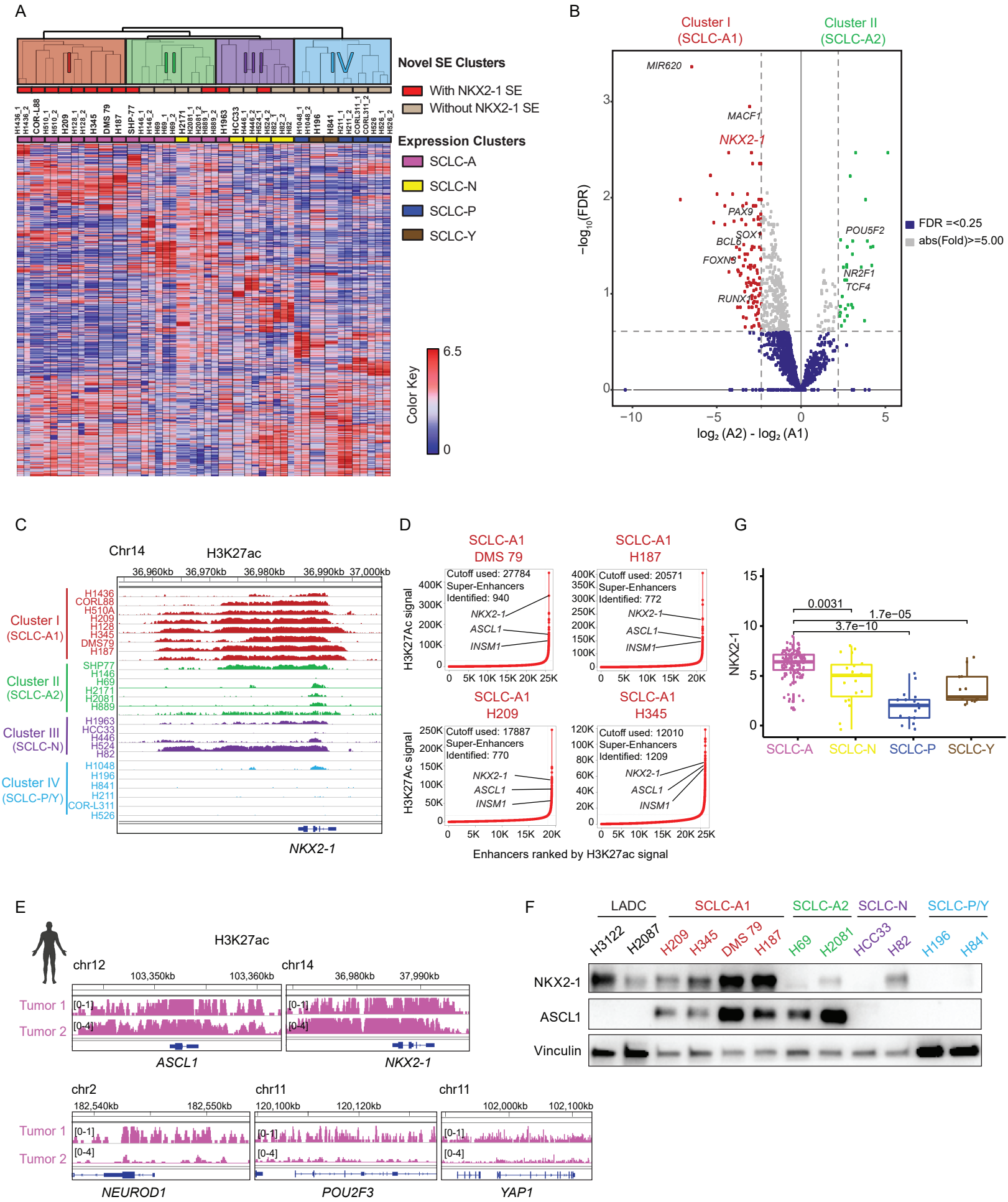
A
Novel SE Clusters
With NKX2-1 SE
Without NKX2-1 SE
Expression Clusters
SCLC-A
SCLC-N
SCLC-P
SCLC-Y
Color Key
6.5
0
B
Cluster I
(SCLC-A1)
Cluster II
(SCLC-A2)
MIR620
MACF1
NKX2-1
PAX9
SOX1
BCL6
FOXN3
RUNX1
POU5F2
NR2F1
TCF4
FDR =<0.25
abs(Fold)>=5.00
−log10(FDR)
log2 (A2) - log2 (A1)
C
Chr14
H3K27ac
36,960kb
36,970kb
36,980kb
36,990kb
37,000kb
Cluster I
(SCLC-A1)
Cluster II
(SCLC-A2)
Cluster III
(SCLC-N)
Cluster IV
(SCLC-P/Y)
NKX2-1
D
SCLC-A1
DMS 79
Cutoff used: 27784
Super-Enhancers
Identified: 940
SCLC-A1
H187
Cutoff used: 20571
Super-Enhancers
Identified: 772
SCLC-A1
H209
Cutoff used: 17887
Super-Enhancers
Identified: 770
SCLC-A1
H345
Cutoff used: 12010
Super-Enhancers
Identified: 1209
NKX2-1
ASCL1
INSM1
H3K27Ac signal
Enhancers ranked by H3K27ac signal
G
NKX2-1
0.0031
1.7e−05
3.7e−10
SCLC-A
SCLC-N
SCLC-P
SCLC-Y
E
H3K27ac
chr12
103,350kb
103,360kb
chr14
36,980kb
37,990kb
Tumor 1
Tumor 2
ASCL1
NKX2-1
chr2
182,540kb
182,550kb
chr11
120,100kb
120,120kb
chr11
102,000kb
102,100kb
NEUROD1
POU2F3
YAP1
F
LADC
SCLC-A1
SCLC-A2
SCLC-N
SCLC-P/Y
H3122
H2087
H209
H345
DMS 79
H187
H69
H2081
HCC33
H82
H196
H841
NKX2-1
ASCL1
Vinculin

Figure 2

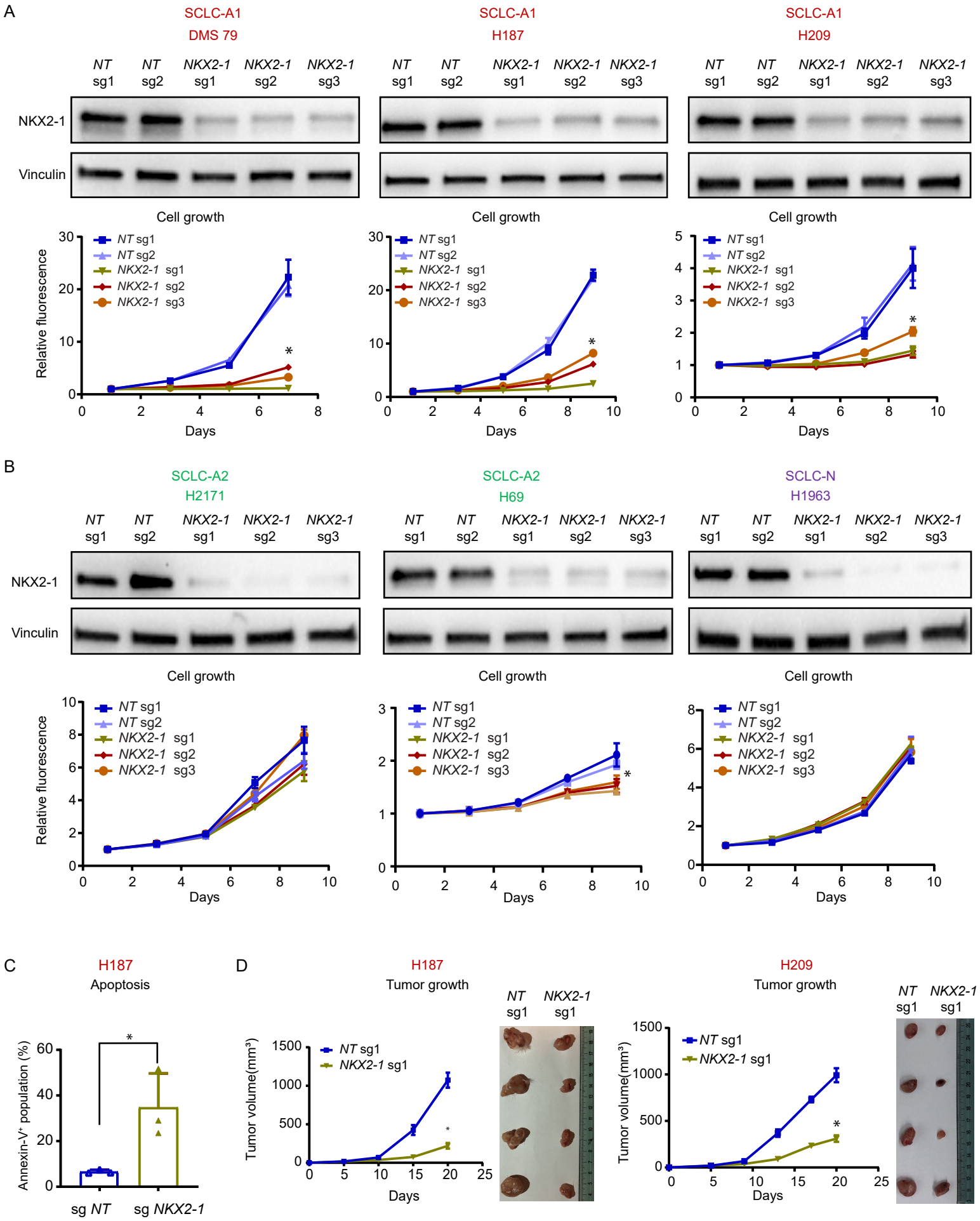
A
SCLC-A1
DMS 79
SCLC-A1
H187
SCLC-A1
H209
NT sg1
NT sg2
NKX2-1 sg1
NKX2-1 sg2
NKX2-1 sg3
NKX2-1
Vinculin
Cell growth
Relative fluorescence
Days
B
SCLC-A2
H2171
SCLC-A2
H69
SCLC-N
H1963
C
H187
Apoptosis
Annexin-V+ population (%)
sg NT
sg NKX2-1
D
H187
Tumor growth
Tumor volume(mm³)
H209
Tumor growth

Figure 3

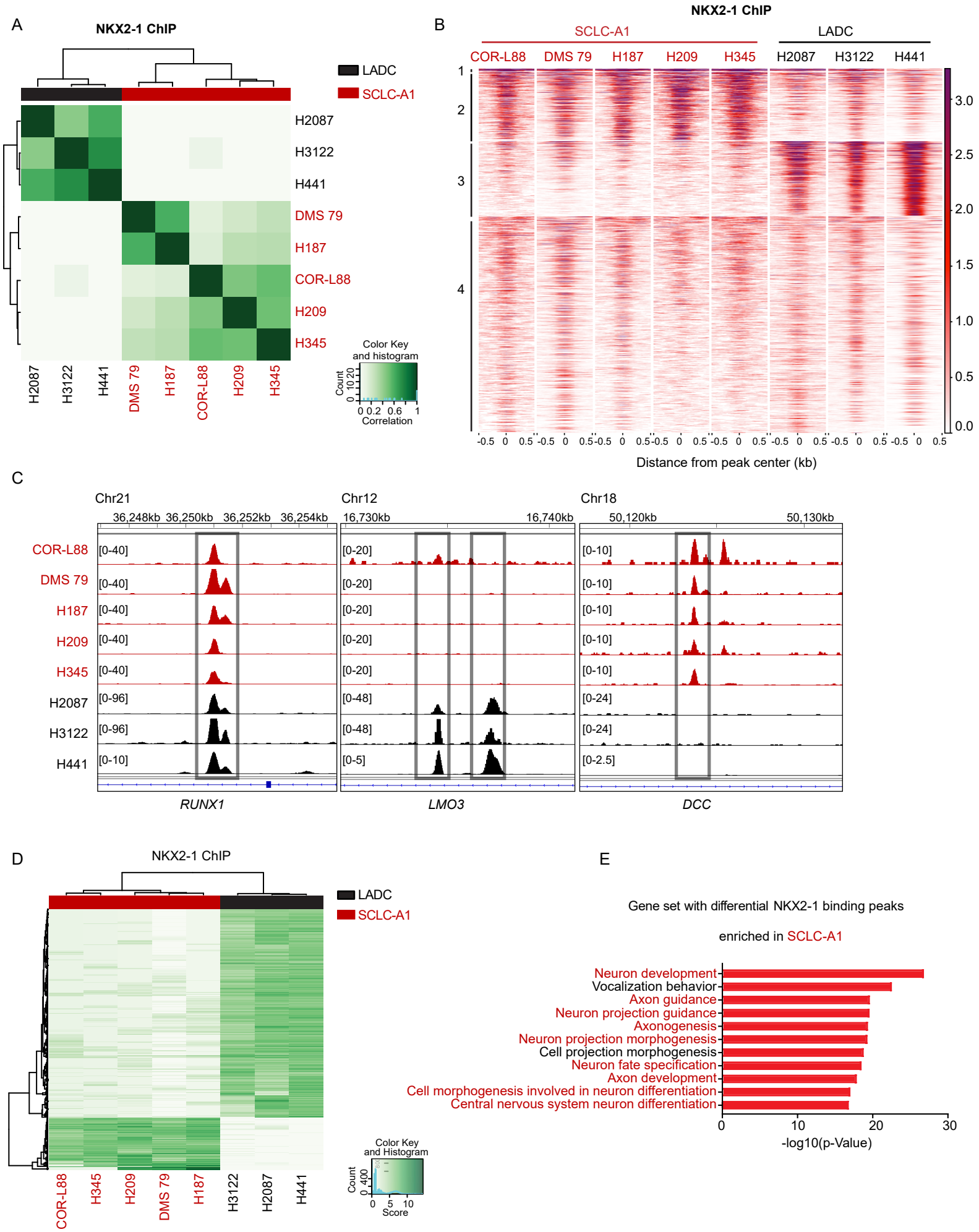
A
NKX2-1 ChIP
LADC
SCLC-A1
H2087
H3122
H441
DMS 79
H187
COR-L88
H209
H345
Color Key and histogram
Count
Correlation
B
NKX2-1 ChIP
SCLC-A1
LADC
COR-L88
DMS 79
H187
H209
H345
H2087
H3122
H441
Distance from peak center (kb)
C
Chr21
Chr12
Chr18
36,248kb 36,250kb 36,252kb 36,254kb
16,730kb
16,740kb
50,120kb
50,130kb
RUNX1
LMO3
DCC
D
NKX2-1 ChIP
LADC
SCLC-A1
Color Key and Histogram
Count
Score
E
Gene set with differential NKX2-1 binding peaks
enriched in SCLC-A1
Neuron development
Vocalization behavior
Axon guidance
Neuron projection guidance
Axonogenesis
Neuron projection morphogenesis
Cell projection morphogenesis
Neuron fate specification
Axon development
Cell morphogenesis involved in neuron differentiation
Central nervous system neuron differentiation
-log10(p-Value)

Figure 4

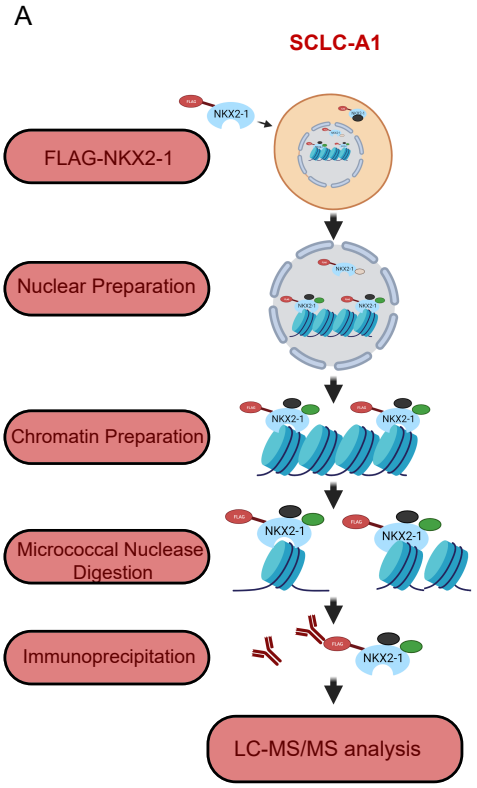
A
SCLC-A1
FLAG-NKX2-1
Nuclear Preparation
Chromatin Preparation
Micrococcal Nuclease Digestion
Immunoprecipitation
LC-MS/MS analysis
NKX2-1

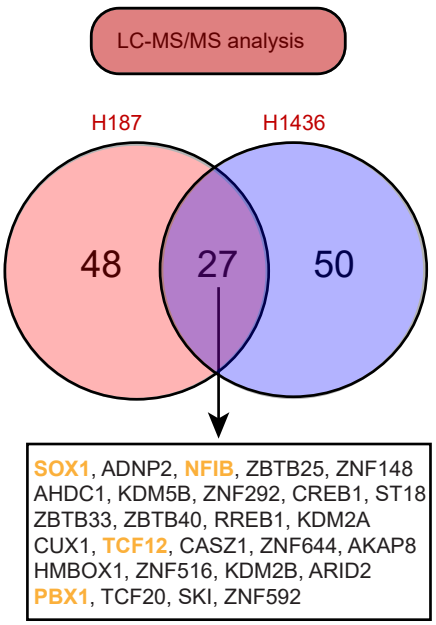
B
LC-MS/MS analysis
H187
H1436
48
27
50
SOX1, ADNP2, NFIB, ZBTB25, ZNF148
AHDC1, KDM5B, ZNF292, CREB1, ST18
ZBTB33, ZBTB40, RREB1, KDM2A
CUX1, TCF12, CASZ1, ZNF644, AKAP8
HMBOX1, ZNF516, KDM2B, ARID2
PBX1, TCF20, SKI, ZNF592

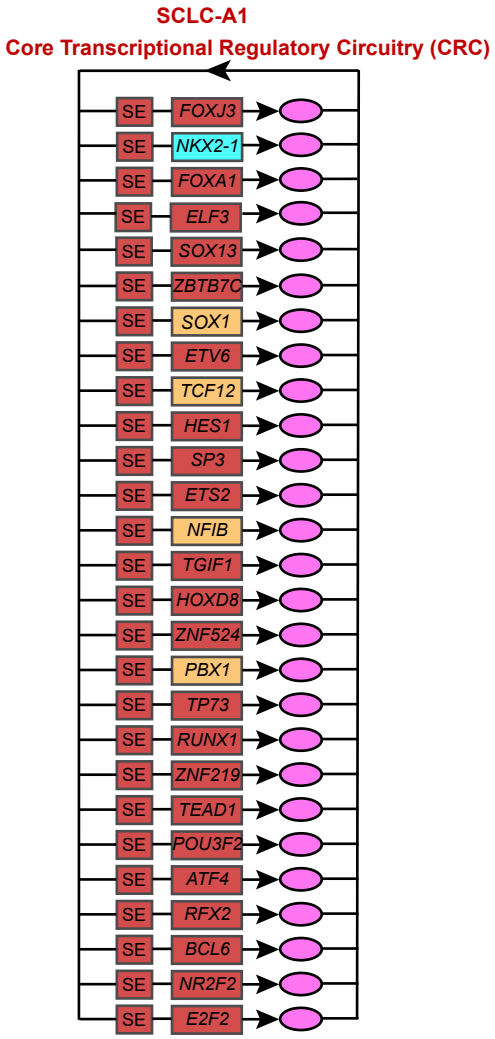
C
SCLC-A1
Core Transcriptional Regulatory Circuitry (CRC)
SE FOXJ3
SE NKX2-1
SE FOXA1
SE ELF3
SE SOX13
SE ZBTB7C
SE SOX1
SE ETV6
SE TCF12
SE HES1
SE SP3
SE ETS2
SE NFIB
SE TGIF1
SE HOXD8
SE ZNF524
SE PBX1
SE TP73
SE RUNX1
SE ZNF219
SE TEAD1
SE POU3F2
SE ATF4
SE RFX2
SE BCL6
SE NR2F2
SE E2F2

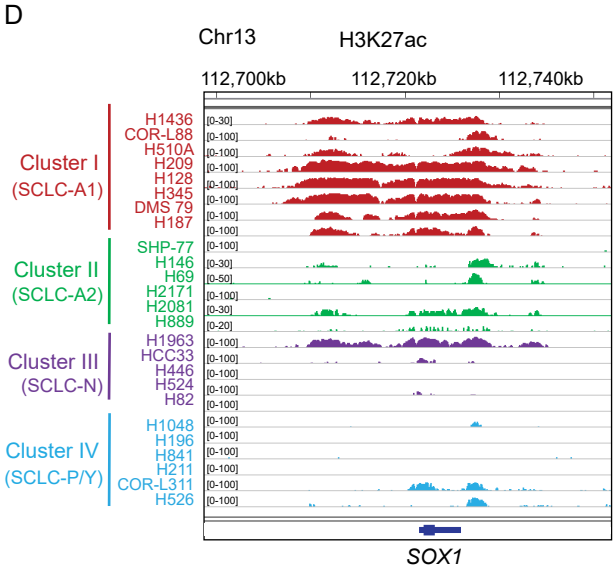
D
Chr13
H3K27ac
112,700kb
112,720kb
112,740kb
Cluster I (SCLC-A1)
H1436
COR-L88
H510A
H209
H128
H345
DMS 79
H187
Cluster II (SCLC-A2)
SHP-77
H146
H69
H2171
H2081
H889
Cluster III (SCLC-N)
H1963
HCC33
H446
H524
H82
Cluster IV (SCLC-P/Y)
H1048
H196
H841
H211
COR-L311
H526
SOX1

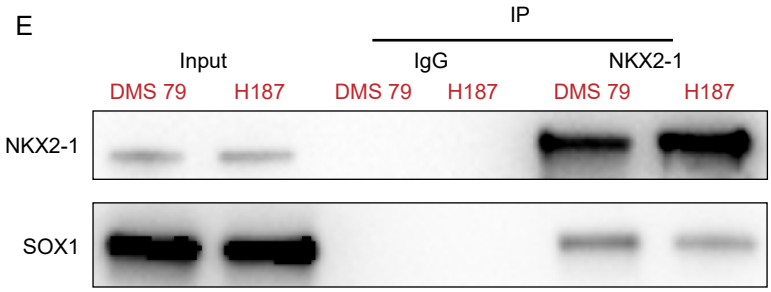
E
IP
Input
IgG
NKX2-1
DMS 79
H187
DMS 79
H187
DMS 79
H187
NKX2-1
SOX1

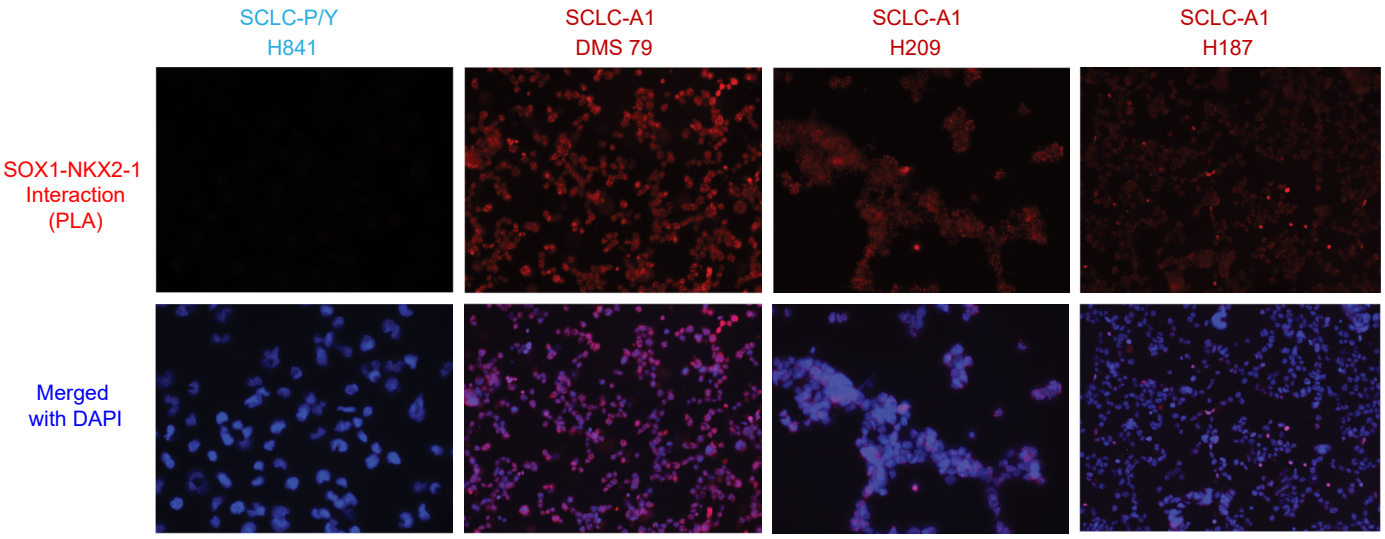
F
SCLC-P/Y
H841
SCLC-A1
DMS 79
SCLC-A1
H209
SCLC-A1
H187
SOX1-NKX2-1 Interaction (PLA)
Merged with DAPI

Figure 5

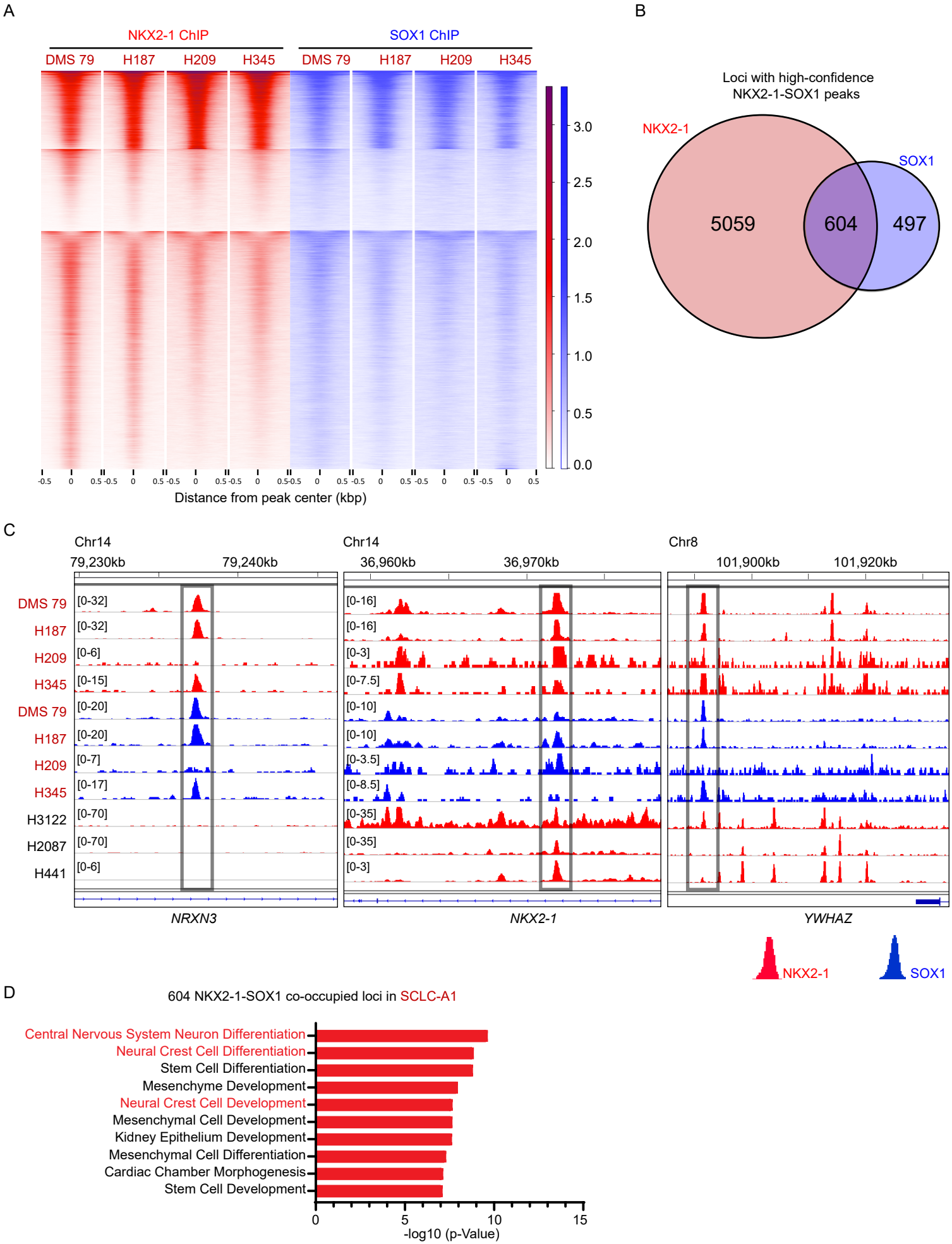
A
NKX2-1 ChIP
SOX1 ChIP
DMS 79
H187
H209
H345
DMS 79
H187
H209
H345
3.0
2.5
2.0
1.5
1.0
0.5
0.0
-0.5
0
0.5
Distance from peak center (kbp)
B
Loci with high-confidence
NKX2-1-SOX1 peaks
NKX2-1
SOX1
5059
604
497
C
Chr14
79,230kb
79,240kb
Chr14
36,960kb
36,970kb
Chr8
101,900kb
101,920kb
DMS 79
H187
H209
H345
DMS 79
H187
H209
H345
H3122
H2087
H441
[0-32]
[0-32]
[0-6]
[0-15]
[0-20]
[0-20]
[0-7]
[0-17]
[0-70]
[0-70]
[0-6]
[0-16]
[0-16]
[0-3]
[0-7.5]
[0-10]
[0-10]
[0-3.5]
[0-8.5]
[0-35]
[0-35]
[0-3]
NRXN3
NKX2-1
YWHAZ
NKX2-1
SOX1
D
604 NKX2-1-SOX1 co-occupied loci in SCLC-A1
Central Nervous System Neuron Differentiation
Neural Crest Cell Differentiation
Stem Cell Differentiation
Mesenchyme Development
Neural Crest Cell Development
Mesenchymal Cell Development
Kidney Epithelium Development
Mesenchymal Cell Differentiation
Cardiac Chamber Morphogenesis
Stem Cell Development
0
5
10
15
-log10 (p-Value)

Figure 6

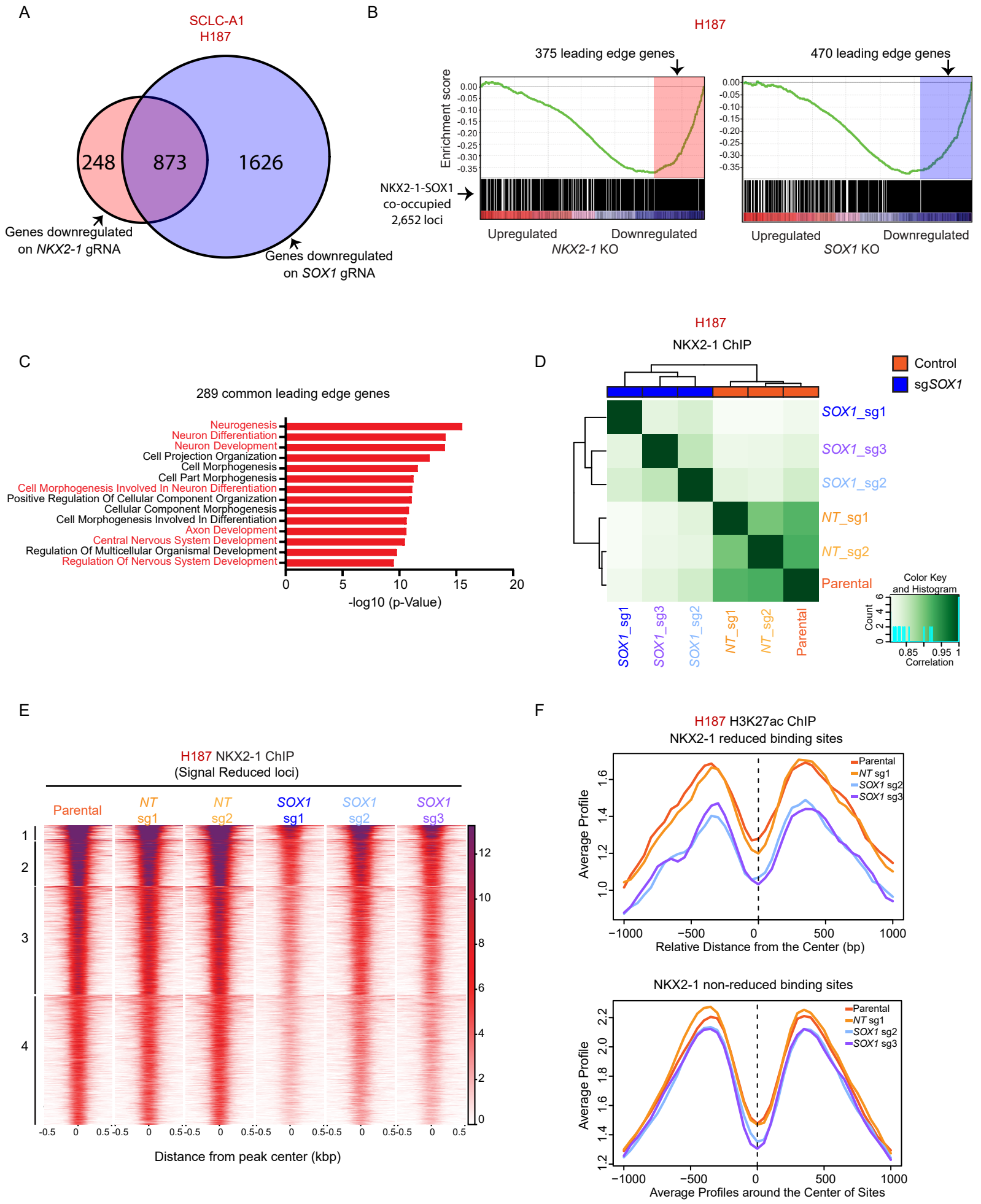
A
SCLC-A1
H187
248
873
1626
Genes downregulated on NKX2-1 gRNA
Genes downregulated on SOX1 gRNA
B
H187
375 leading edge genes
470 leading edge genes
Enrichment score
NKX2-1-SOX1 co-occupied 2,652 loci
Upregulated
Downregulated
NKX2-1 KO
SOX1 KO
C
289 common leading edge genes
Neurogenesis
Neuron Differentiation
Neuron Development
Cell Projection Organization
Cell Morphogenesis
Cell Part Morphogenesis
Cell Morphogenesis Involved In Neuron Differentiation
Positive Regulation Of Cellular Component Organization
Cellular Component Morphogenesis
Cell Morphogenesis Involved In Differentiation
Axon Development
Central Nervous System Development
Regulation Of Multicellular Organismal Development
Regulation Of Nervous System Development
-log10 (p-Value)
D
H187
NKX2-1 ChIP
Control
sgSOX1
SOX1_sg1
SOX1_sg3
SOX1_sg2
NT_sg1
NT_sg2
Parental
Color Key and Histogram
Count
Correlation
E
H187 NKX2-1 ChIP
(Signal Reduced loci)
Parental
NT sg1
NT sg2
SOX1 sg1
SOX1 sg2
SOX1 sg3
Distance from peak center (kbp)
F
H187 H3K27ac ChIP
NKX2-1 reduced binding sites
Parental
NT sg1
SOX1 sg2
SOX1 sg3
Average Profile
Relative Distance from the Center (bp)
NKX2-1 non-reduced binding sites
Average Profiles around the Center of Sites

Figure 7

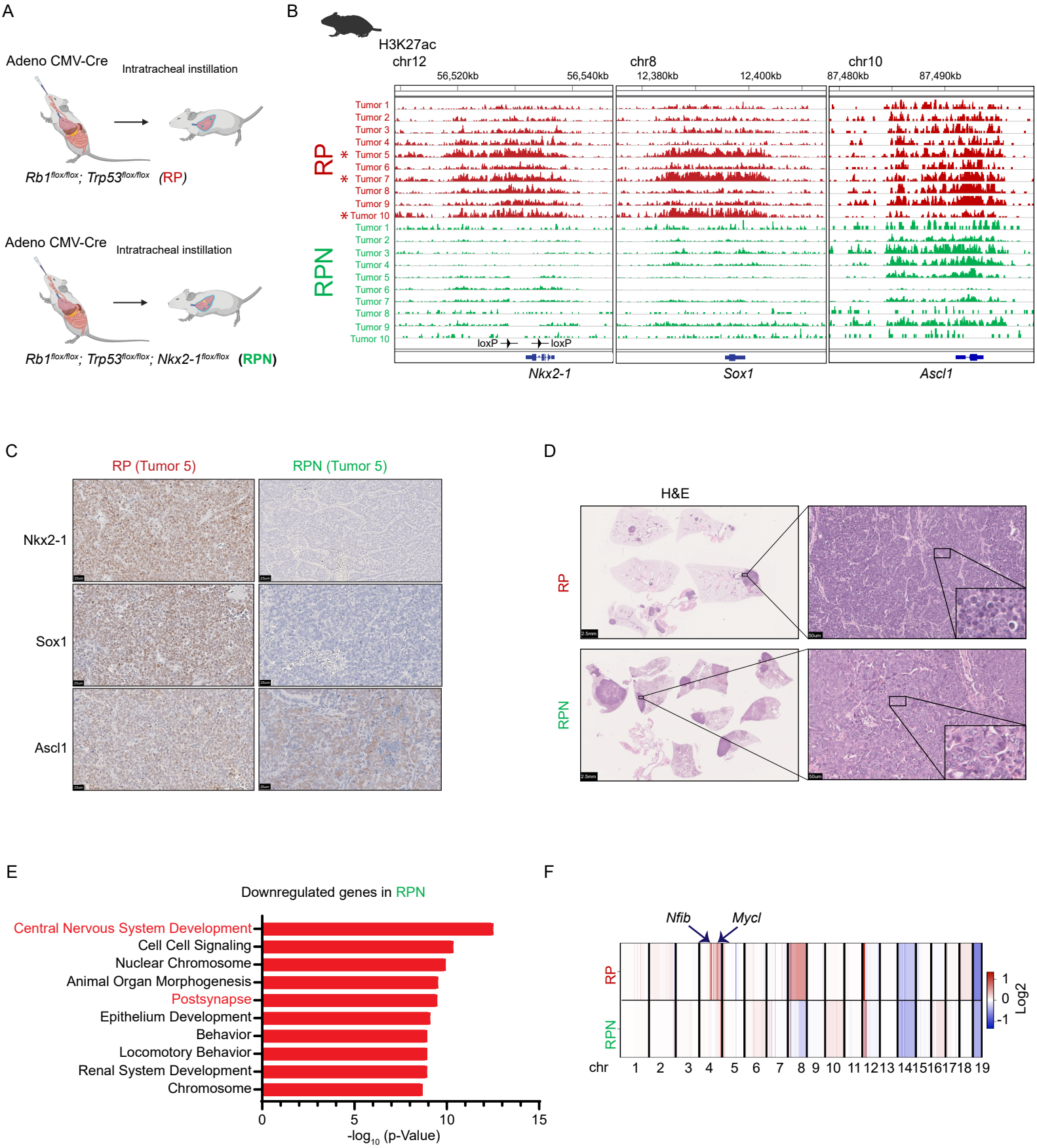
A
Adeno CMV-Cre
Intratracheal instillation
Rb1flox/flox; Trp53flox/flox (RP)
Adeno CMV-Cre
Intratracheal instillation
Rb1flox/flox; Trp53flox/flox; Nkx2-1flox/flox (RPN)
B
H3K27ac
chr12
56,520kb
56,540kb
chr8
12,380kb
12,400kb
chr10
87,480kb
87,490kb
RP
Tumor 1
Tumor 2
Tumor 3
Tumor 4
Tumor 5
Tumor 6
Tumor 7
Tumor 8
Tumor 9
Tumor 10
RPN
Tumor 1
Tumor 2
Tumor 3
Tumor 4
Tumor 5
Tumor 6
Tumor 7
Tumor 8
Tumor 9
Tumor 10
loxP
loxP
Nkx2-1
Sox1
Ascl1
C
RP (Tumor 5)
RPN (Tumor 5)
Nkx2-1
Sox1
Ascl1
D
H&E
RP
RPN
E
Downregulated genes in RPN
Central Nervous System Development
Cell Cell Signaling
Nuclear Chromosome
Animal Organ Morphogenesis
Postsynapse
Epithelium Development
Behavior
Locomotory Behavior
Renal System Development
Chromosome
0
5
10
15
-log10 (p-Value)
F
Nfib
Mycl
RP
RPN
chr
1 2 3 4 5 6 7 8 9 10 11 12 13 14 15 16 17 18 19
1
0
-1
Log2